CrossMark

Analysis of X-Ray Emission from OB Stars. IV. About X-Ray Emission from Inhomogeneous Winds of OB Stars

Elizaveta Ryspaeva[1,2] and Alexander Kholtygin[2]
[1] Crimean Astrophysical Observatory, Nauchny, Crimea, Russia; e.ryspaeva@yandex.ru
[2] Saint-Petersburg State University, Saint-Petersburg, Russia; afkholtygin@gmail.com

Abstract

We study the origin of X-ray emission from OB stars due to collisions of stellar winds and/or inhomogeneities in the winds. The low-resolution X-ray spectra of a big sample of OB stars were fitted by both the stationary APEC/MEKAL models and by this model with an additional PSHOCK component describing the nonstationary X-ray emission. These spectra were also described by two-temperature PSHOCK models. More than $\sim 50\%$ of considered spectra can be described by the above-mentioned model combinations including the PSHOCK model and the quality of the fits appears to be better for O stars. The plasma temperature of the PSHOCK component is about 1–5 keV with the ionization timescale $\tau_u \sim 10^8$–10^{13} s cm^{-3}. The temperature of the PSHOCK component increases with the momentum and kinetic energy of the stellar wind by a power law with an index ~ 0.12–0.14. Such dependencies were not revealed through modeling by the stationary APEC/MEKAL models only. At the same time the X-ray luminosity of OB stars depends on momentum and kinetic energy of their winds similarly either for stationary or for nonstationary models. We conclude that many O stars and some B stars can be sources of the nonstationary X-rays formed in their inhomogeneous stellar wind.

Key words: stars: early-type – stars: statistics – X-rays: stars

1. Introduction

The X-ray emission from strongly magnetic OB stars is usually considered in a framework of the Magnetically Confined Wind Shock Model (MCWS) by Babel & Montmerle (1997) (see also ud-Doula & Owocki 2002). In this model the X-ray emission is produced in the postshock region by low density hot plasma. ud-Doula et al. (2014), ud-Doula & Nazé (2016), Ryspaeva & Kholtygin (2020) inferred possible consequences from the MCWS: the temperature of X-rays emitted by the plasma should increase with the hardness ratio, the terminal wind velocity, the mass loss rate and the magnetic field. Ryspaeva & Kholtygin (2020) checked if these consequences are valid for a big sample of X-ray spectra from OB stars but did not confirm them. Moreover the MCWS cannot explain the formation of X-rays from weakly magnetic OB stars.

Alternatively, X-ray emission from OB stars can be generated due to instability in the radiative stellar winds or as a result of the wind's collisions in binary or multiple systems. The first model of stellar X-rays resulting from the collision of winds in double stars was proposed by Cherepashchuk (1976). Lucy & White (1980) developed a first model of X-ray emission arising from radiation instability in winds from OB stars. Antokhin et al. (1988) argued that the winds from early-type stars are inhomogeneous and contain blobs (clumps) surrounded by less dense gas.

Detailed one-dimensional hydrodynamic models (Owocki et al. 1988; Runacres & Owocki 2002 and references therein) explain the generation of X-rays from single OB stars as a result of shocks formed due to instability inherent in radiation-induced stellar winds (Lucy & White 1980; Lucy 1982).

Taking into account the existence of inhomogeneities in the stellar winds, Hillier et al. (1993), Feldmeier et al. (1997) supplemented the hydrodynamic model describing the X-rays from stars and supposed that the X-ray emission is generated at a distance of several stellar radii from the stellar surface when fast gas blobs pass through a slower moving ambient gas (see also Oskinova 2016). This model predicted the variability of the stellar X-rays on a timescale of up to a few days.

Cassinelli et al. (2008), Ignace et al. (2012) calculated temperatures and densities in shock waves arising during the propagation of blobs in stellar winds. The authors estimated the power distribution of the emission measure obtained from the analysis of observations and a wide range of ionization stages of atoms that are present in stellar winds. Cassinelli & Swank (1983), Waldron & Cassinelli (2009) developed a "hybrid" model explaining the X-ray emission of massive stars by a combination of plasma heating in the regions of local magnetic fields during reconnection of magnetic field lines and heating by shock waves in the stellar winds.

In the hot plasma of the OB star winds, the cooling and recombination times are small (minutes or even seconds). It

Table 1
The List of Additional Objects, their Parameters and Log of Observation

Star	Sp.Type	$E(B-V)$ (mag)	d (pc)	ObsID	Date	Exposure, (s)
ALS18058	B9V	0.195	291	201 550 201	2004-02-13	43 611
BD+433654	O4If C	1.275	1651	653 690 101	2010-05-08	46 715
HD 17505	O6.5III((f))n+O8V	0.71	877	840 910 101	2020-02-02	11 200
HD 18552	B7IVe	0.041	228	820 310 901	2018-08-29	15 000
HD 24398	B1Ib	0.273	230	201 550 201	2004-02-13	43 611
HD 36408	B7III	0.292	917	820 311 001	2019-03-20	24 600
HD 43285	B6Ve	0.016	224	820 310 801	2019-03-30	11 800
HD 83953	B5V C	0.015	155	820 310 701	2018-06-10	16 400
HD 97434	O7.5III(n)((f))	0.390	2755	51 550 101	2002-02-06	40 822
				760 330 101	2015-06-14	88 900
HD 200120	B1.5Vnne	0.076	399	820 310 501	2018-05-17	14 000
HD 219688	B7/8V	0.09	123	820 311 101	2018-06-14	19 200
HD 287848	B8 E	0.03	362	554 610 101	2009-03-01	63 916
HD 287849	B3 E	0.033	379	554 610 101	2009-03-01	63 916

Table 2
Parameters of Best Spectral Fits by Sums of APEC/MEKAL Models

Star	$N_{\mathrm{H}}^{\mathrm{local}}$ 10^{22} cm^{-2}	kT_1 keV	$\log EM_1$ cm^{-3}	$kT_{2,3}$ keV	$\log EM_{2,3}$ cm^{-3}	Abund. sol. un.	χ^2 (d.o.f.)
ALS18058	0.12 ± 0.07	0.27 ± 0.03	53.78 ± 0.28	1.12 ± 0.13	53.21 ± 0.11	0.23 ± 0.09	1.12 (253)
BD+433654	1.07 ± 0.10	0.25 ± 0.07	55.84 ± 0.56	0.69 ± 0.12	54.96 ± 0.42	0.67 ± 0.67	0.89 (308)
HD 17505	0.39 ± 0.08	0.22 ± 0.03	56.02 ± 0.31	1.59 ± 0.25	54.65 ± 0.06	1.0	0.96 (304)
HD 18552	<0.006	0.12 ± 0.03	52.64 ± 0.38	0.67 ± 0.03	52.57 ± 0.05	1.0	1.09 (255)
				1.65 ± 0.18	52.72 ± 0.06		
HD 24398	0.06 ± 0.06	0.17 ± 0.02	54.33 ± 0.20	0.61 ± 0.03	53.89 ± 0.09	0.36 ± 0.13	1.01 (259)
HD 43285	<0.024	0.32 ± 0.03	52.18 ± 0.09	1.45 ± 0.16	52.12 ± 0.09	1.0	0.85 (151)
HD 83953	<0.011	0.84 ± 0.28	52.08 ± 0.19	1.80 ± 0.22	53.14 ± 0.07	0.27 ± 0.09	1.18 (347)
HD 97434	0.09 ± 0.05	0.15 ± 0.01	55.25 ± 0.23	0.61 ± 0.04	54.62 ± 0.08	1.0	0.98 (316)
HD 200120	1.22 (fr.)	0.15 ± 0.05	52.79 ± 0.26	0.50 ± 0.21	52.24 ± 0.23	1.0	0.86 (101)
HD 219688†	<0.049	0.24 ± 0.04	52.13 ± 0.24	0.92 ± 0.08	52.09 ± 0.19	0.31 ± 0.16	0.82 (224)
HD 287848	<0.020	0.66 ± 0.03	53.18 ± 0.11	1.30 ± 0.10	53.31 ± 0.07	0.39 ± 0.09	1.17 (349)
HD 287849	<0.017	0.23 ± 0.04	52.28 ± 0.13	0.88 ± 0.06	52.47 ± 0.05	1.0	1.02 (298)
				2.69 ± 0.61	52.57 ± 0.08		

Note. Stars with no estimated local $N_{\mathrm{H}}^{\mathrm{local}}$ are marked by $\dagger$. Parameters kT_3 and $\log EM_3$ for HD 18552 and HD 287849 are given below the kT_2 and $\log EM_2$ values. The symbols (fr.) mark the fixed parameter values.

means that nonstationary models of X-ray formation are preferable to stationary ones. In the present paper we study possible nonstationary stellar X-rays, which can be generated by collisions of stellar winds or by inhomogeneities in the winds, and/or by plasma heating in local magnetic fields. For this we fit X-ray spectra of a big sample of OB stars by models with a PSHOCK component.

Our paper is organized in the following manner. Section 2 describes observations used in our work and their reduction. The results of spectral analysis are presented in Section 3. The possible dependences between characteristics of stellar X-ray emission are analyzed in Section 4. The discussion and general conclusion are given in Section 5.

2. Observations and Data Reduction

We analyze archival X-ray observations of 40 O stars and 44 B stars, obtained by the "XMM-Newton" space observatory; 71 targets have been already considered in our previous papers by Ryspaeva & Kholtygin (2018, 2019, 2020).[3] The list of additional targets, their parameters (spectral type, color excess, distance) and log of observation is given in Table 1. The distances to the stars are calculated by parallaxes from the Gaia Data Release 2 (DR2) online catalog (2018).[4] Color excesses

---

[3] Lists of studied stars and their parameters are given in Table 1 in these papers.

[4] http://vizier.u-strasbg.fr/viz-bin/VizieR?-source=I/345

Table 3
The Same as in Table 2, but for Best Spectral Fits by APEC/MEKAL+PSHOCK Models

Star	N_{H} 10^{22} cm^{-2}	$kT_{1,2}$ keV	$\log EM_{1,2}$ cm^{-3}	kT_{shock} keV	$\log EM_{\mathrm{shock}}$ cm^{-3}	τ_u 10^{11} s cm^{-3}	Abund. sol. un.	χ^2 (d.o.f.)
ALS18058	0.09 ± 0.06	0.56 ± 0.09	54.37 ± 0.19	3.10 ± 1.12	53.64 ± 0.21	0.088 ± 0.053	0.17 ± 0.06	1.09 (252)
BD-145040	0.59 ± 0.03	0.49 ± 0.15	52.80 ± 0.16	0.73 ± 0.40	53.08 ± 0.08	0.26 ± 0.24	1.91 ± 0.24	0.98 (137)
BD+433654	0.57 ± 0.07	1.00 ± 0.34	53.40 ± 0.40	1.00 ± 0.11	53.66 ± 0.08	1.00 ± 0.55	1.00 ± 0.12	1.06 (307)
CPD-282561	0.46 ± 0.11	0.72 ± 0.17	52.79 ± 0.30	3.05 ± 0.78	52.99 ± 0.09	11.98 ± 10.96	0.32 ± 0.19	1.07 (319)
HD 108	<0.013	2.10 ± 0.11	55.20 ± 0.03	0.78 ± 0.02	55.08 ± 0.09	8.72 ± 3.22	0.45 ± 0.09	1.25 (405)
HD 10144	0.08 (fr.)	0.56 ± 0.07	53.67 ± 0.27	0.43 ± 0.22	53.34 ± 0.50	4.26 ± 4.14	0.89 ± 0.55	1.15 (204)
HD 15558	0.02 ± 0.05	0.53 ± 0.06	56.05 ± 0.16	2.01 ± 0.28	55.71 ± 0.10	0.63 ± 0.16	0.20 ± 0.05	1.16 (382)
HD 15570	0.26 ± 0.07	0.58 ± 0.05	52.86 ± 0.11	0.65 ± 0.09	53.50 ± 0.15	$(8.85 \pm 3.51) \cdot 10^{-3}$	1.0	1.3 (281)
HD 17505	0.43 (fr.)	0.80 ± 0.05	54.48 ± 0.11	2.24 ± 0.86	53.82 ± 0.16	0.16 ± 0.09	0.25 ± 0.06	0.9 (303)
HD 18552[†]	<0.01	1.32 ± 0.26	54.96 ± 0.20	0.77 ± 0.14	54.79 ± 0.21	10.05 ± 5.88	0.32 ± 0.13	1.06 (255)
HD 24398	<0.080	0.12 ± 0.03	56.41 ± 0.47	0.64 ± 0.04	55.82 ± 0.08	6.49 ± 2.70	0.34 ± 0.09	0.97 (258)
HD 24760	0.11 ± 0.07	0.29 ± 0.02 3.04 ± 1.59	54.09 ± 0.18 52.88 ± 0.21	0.19 ± 0.05	55.64 ± 0.28	$(2.61 \pm 1.44) \cdot 10^{-3}$	1.0	0.9 (190)
HD 33904	0.06 ± 0.01	0.30 ± 0.01 1.01 ± 0.02	54.48 ± 0.03 54.46 ± 0.02	1.68 ± 0.16	54.75 ± 0.05	$(2.24 \pm 0.36) \cdot 10^{-3}$	1.0	1.56 (400)
HD 34078	0.12 ± 0.04	0.30 ± 0.03	55.43 ± 0.18	0.32 ± 0.06	55.66 ± 0.27	1.54 ± 0.78	1.0	1.37 (300)
HD 37479	<0.01	0.74 ± 0.10	52.95 ± 0.31	4.38 ± 0.75	53.38 ± 0.04	4.59 ± 2.86	0.16 ± 0.09	1.29 (254)
HD 47129	0.08 ± 0.03	0.62 ± 0.01 2.07 ± 0.18	55.77 ± 0.06 55.71 ± 0.06	1.86 ± 0.38	55.81 ± 0.10	$(5.92 \pm 1.63) \cdot 10^{-3}$	1.0	1.33 (416)
HD 47839	0.04 (fr.)	0.11 ± 0.00 0.27 ± 0.01	55.26 ± 0.05 54.68 ± 0.05	0.97 ± 0.11	53.87 ± 0.06	1.58 ± 0.68	1.0	1.72 (239)
HD 54662	<0.087	0.53 ± 0.06	53.65 ± 0.19	0.33 ± 0.12	53.89 ± 0.49	16.43 ± 15.68	0.48 ± 0.18	0.94 (257)
HD 54879	0.07 ± 0.07	0.13 ± 0.05	54.89 ± 0.62	0.74 ± 0.04	54.54 ± 0.09	6.34 ± 3.57	0.42 ± 0.15	1.05 (306)
HD 57682	<0.029	1.23 ± 0.28	54.31 ± 0.22	0.75 ± 0.11	54.26 ± 0.21	30.76 ± 24.85	0.31 ± 0.14	0.95 (277)
HD 63922	0.05 ± 0.03	0.10 ± 0.01 0.26 ± 0.01	56.43 ± 0.31 55.68 ± 0.11	0.89 ± 0.08	54.61 ± 0.08	16.81 ± 14.52	1.0	1.13 (328)
HD 64760	<0.05	0.12 ± 0.03	56.11 ± 0.43	0.76 ± 0.02	55.52 ± 0.05	4.21 ± 1.03	0.21 ± 0.03	1.31 (358)
HD 83953	<0.01	0.69 ± 0.34	54.20 ± 0.45	2.10 ± 0.25	55.73 ± 0.06	20.27 ± 11.87	0.30 ± 0.11	1.15 (346)
HD 93128	0.29 ± 0.05	2.17 ± 0.37	54.36 ± 0.09	0.71 ± 0.09	54.38 ± 0.27	2.69 ± 1.25	0.29 ± 0.15	0.99 (233)
HD 93129	0.38 ± 0.02	0.61 ± 0.02	54.55 ± 0.05	2.75 ± 0.18	53.96 ± 0.03	0.075 ± 0.015	0.10 ± 0.01	1.89 (466)
HD 93205	<0.010	0.47 ± 0.06	55.38 ± 0.11	1.65 ± 0.25	55.13 ± 0.09	0.85 ± 0.18	0.29 ± 0.06	1.3 (389)
HD 93250	0.38 ± 0.05	0.24 ± 0.01	53.40 ± 0.13	2.76 ± 0.42	52.46 ± 0.06	6.34 ± 2.80	1.0	1.84 (299)
HD 93403	0.11 ± 0.02	1.51 ± 0.06	56.25 ± 0.03	0.76 ± 0.02	56.32 ± 0.06	4.88 ± 1.04	0.41 ± 0.05	1.31 (423)
HD 93521	0.16 ± 0.04	0.14 ± 0.02 0.41 ± 0.09	52.86 ± 0.54 52.22 ± 0.06	3.68 ± 0.14	52.00 ± 0.07	$(6.18 \pm 1.86) \cdot 10^{-3}$	1.0	0.8 (254)
HD 97434	0.02 ± 0.15	0.09 ± 0.02	52.77 ± 0.89	0.60 ± 0.07	51.23 ± 0.12	5.55 ± 2.27	1.0	0.96 (315)
HD 101205	0.26 ± 0.04	0.16 ± 0.01 0.60 ± 0.02	56.00 ± 0.18 55.18 ± 0.07	2.24 ± 0.36	54.61 ± 0.06	2.55 ± 1.05	1.0	1.23 (368)
HD 120324	<0.014	1.15 ± 0.21	53.84 ± 0.18	0.61 ± 0.17	53.67 ± 0.24	3.92 ± 2.52	0.34 ± 0.18	1.13 (205)
HD 144217[†]	0.06 ± 0.08	0.58 ± 0.01	53.88 ± 0.04	2.29 ± 0.28	53.43 ± 0.04	0.086 ± 0.010	0.36 ± 0.03	1.4 (401)
HD 148937	0.03 ± 0.03	0.60 ± 0.02 1.20 ± 0.04	56.86 ± 0.07 56.77 ± 0.07	2.98 ± 0.31	56.73 ± 0.06	$(1.02 \pm 0.22) \cdot 10^{-2}$	0.45 ± 0.09	1.62 (477)
HD 152233	0.33 ± 0.03	0.56 ± 0.02	55.63 ± 0.08	0.17 ± 0.01	56.58 ± 0.11	4.98 ± 2.72	0.67 ± 0.16	1.8 (353)
HD 152234	0.04 ± 0.02	0.16 ± 0.02 0.54 ± 0.05	55.03 ± 0.16 54.89 ± 0.06	1.40 ± 0.22	54.41 ± 0.14	1.28 ± 0.34	0.45 ± 0.08	1.49 (383)
HD 152249	0.15 ± 0.01	0.48 ± 0.03	51.57 ± 0.08	2.96 ± 0.39	51.16 ± 0.06	0.049 ± 0.012	1.0	1.39 (405)
HD 155806	0.01 ± 0.82	0.53 ± 0.04	52.51 ± 0.20	0.36 ± 0.04	52.60 ± 0.27	1.00 ± 0.51	0.67 ± 0.28	1.05 (302)
HD 157246	0.26 ± 0.03	0.06 ± 0.01	57.08 ± 0.50	0.68 ± 0.04	54.68 ± 0.04	4.89 ± 1.38	1.0	1.27 (293)
HD 159176	0.04 ± 0.03	0.24 ± 0.02 0.69 ± 0.07	55.96 ± 0.15 55.70 ± 0.06	3.18 ± 1.12	54.34 ± 0.18	1.78 ± 0.95	0.20 ± 0.04	1.14 (326)
HD 167971	0.03 ± 0.03	1.54 ± 0.07	55.96 ± 0.04	0.72 ± 0.03	56.21 ± 0.06	3.60 ± 0.83	0.58 ± 0.08	1.41 (410)
HD 191612	<0.007	0.71 ± 0.02	55.49 ± 0.06	2.76 ± 0.18	55.28 ± 0.02	3.12 ± 0.89	0.22 ± 0.03	1.36 (459)
HD 193924	<0.008	0.58 ± 0.03	54.14 ± 0.12	0.56 ± 0.45	53.31 ± 0.75	7.84 ± 7.78	0.40 ± 0.15	0.92 (258)
HD 215835	0.23 ± 0.11	0.26 ± 0.03	55.91 ± 0.29	0.86 ± 0.08	55.10 ± 0.19	10.13 ± 6.57	0.79 ± 0.37	1.14 (265)
HD 287848[†]	<0.003	0.69 ± 0.01	54.19 ± 0.02	1.73 ± 0.10	54.41 ± 0.03	95.68 ± 67.18	1.0	1.32 (349)
HD 287849[†]	<0.01	0.79 ± 0.03	54.06 ± 0.05	5.12 ± 2.18	54.11 ± 0.08	3.31 ± 1.28	1.0	1.09 (299)
Tr16-22	0.18 ± 0.14	1.86 ± 0.22	53.11 ± 0.10	3.02 ± 2.31	52.54 ± 0.28	6.46 ± 6.12	0.66 ± 0.27	0.93 (372)

Note. Parameters kT_2 and $\log EM_2$ for some spectra are given below the kT_1 and $\log EM_1$ values.

Table 4
The Same as in Table 2, but for the Best Spectral Fits by PSHOCK+PSHOCK Models

Star	N_H 10^{22} cm^{-2}	kT_1 keV	$\log EM_1$ cm^{-3}	kT_2 keV	$\log EM_2$ cm^{-3}	τ_u 10^{11} s cm^{-3}	Abund. sol. un.	χ^2 (d.o.f.)
ALS18058	<0.051	0.68 ± 0.13	52.84 ± 0.24	2.64 ± 0.99	52.74 ± 0.16	3.07 ± 1.38	0.36 ± 0.17	1.07 (252)
BD+433654	0.96 ± 0.11	0.26 ± 0.09	56.32 ± 0.60	0.72 ± 0.16	55.35 ± 0.29	28.34 ± 24.59	1.0	0.88 (308)
CPD-282561	0.73 ± 0.36	0.50 ± 0.31	56.49 ± 0.83	2.63 ± 0.71	55.54 ± 0.15	3.10 ± 1.89	0.56 ± 0.30	1.06 (319)
HD 108	0.51 ± 0.03	0.27 ± 0.01	57.00 ± 0.14	2.20 ± 0.29	55.90 ± 0.06	5.30 ± 2.93	0.70 ± 0.18	1.52 (405)
HD 10144	<0.045	0.14 ± 0.06	51.78 ± 0.84	0.70 ± 0.06	51.36 ± 0.08	6.24 ± 2.66	1.0	1.14 (204)
HD 15558	<0.11	0.73 ± 0.08	55.51 ± 0.10	2.90 ± 0.62	54.95 ± 0.12	2.11 ± 0.77	0.30 ± 0.06	1.13 (382)
HD 15570	0.34 ± 0.11	0.25 ± 0.08	56.25 ± 0.46	0.79 ± 0.08	55.62 ± 0.14	10.64 ± 7.87	0.24 ± 0.08	1.23 (278)
HD 17505	<0.028	0.73 ± 0.09	54.98 ± 0.17	2.90 ± 1.17	54.25 ± 0.34	3.14 ± 1.22	0.29 ± 0.09	0.9 (302)
HD 18552†	<0.013	0.76 ± 0.17	52.90 ± 0.17	1.35 ± 0.28	52.95 ± 0.22	33.00 ± 23.52	0.28 ± 0.10	1.07 (255)
HD 24398	<0.075	0.15 ± 0.04	54.07 ± 0.48	0.64 ± 0.04	53.82 ± 0.08	6.82 ± 2.88	0.34 ± 0.09	0.98 (258)
HD 36512	<7.5 · 10^{-4}	0.15 ± 0.01	54.04 ± 0.24	0.55 ± 0.02	53.63 ± 0.20	2.17 ± 0.41	1.05 ± 0.45	1.35 (261)
HD 37000	0.77 ± 0.05	0.23 ± 0.03	55.29 ± 0.32	1.59 ± 0.65	53.08 ± 0.22	2.04 ± 1.21	0.43 ± 0.23	1.22 (221)
HD 46328	0.01 ± 0.01	0.13 ± 0.01	54.14 ± 0.08	0.70 ± 0.01	54.13 ± 0.01	5.37 ± 0.36	0.33 ± 0.02	1.96 (402)
HD 47129	0.48 ± 0.03	0.27 ± 0.01	56.35 ± 0.12	2.13 ± 0.12	55.15 ± 0.04	1.73 ± 0.34	0.33 ± 0.06	1.75 (417)
HD 54662	0.03 ± 0.03	0.23 ± 0.02	54.82 ± 0.36	0.59 ± 0.07	54.51 ± 0.25	6.70 ± 3.56	1.14 ± 0.57	0.88 (257)
HD 54879	0.08 ± 0.07	0.17 ± 0.08	54.33 ± 0.46	0.74 ± 0.03	54.63 ± 0.12	7.51 ± 3.63	0.45 ± 0.17	1.06 (306)
HD 57682	<0.02	0.72 ± 0.15	54.94 ± 0.24	1.38 ± 0.38	54.89 ± 0.29	36.99 ± 28.72	0.29 ± 0.13	0.96 (277)
HD 63922	<0.027	0.14 ± 0.01	54.15 ± 0.22	0.58 ± 0.02	53.64 ± 0.04	2.16 ± 0.29	1.0	1.59 (330)
HD 64760	<0.031	0.14 ± 0.03	54.71 ± 0.27	0.76 ± 0.02	54.50 ± 0.05	4.55 ± 1.08	0.20 ± 0.03	1.32 (358)
HD 79351	<6.57 · 10^{-4}	0.73 ± 0.03	53.07 ± 0.04	1.27 ± 0.05	53.14 ± 0.05	44.21 ± 12.18	0.24 ± 0.03	1.4 (416)
HD 83953	<0.013	0.74 ± 0.31	51.51 ± 0.46	2.09 ± 0.24	53.07 ± 0.06	22.77 ± 11.95	0.30 ± 0.11	1.15 (346)
HD 93128	0.32 ± 0.07	0.61 ± 0.10	55.83 ± 0.26	3.14 ± 0.90	55.41 ± 0.13	3.43 ± 1.75	0.18 ± 0.08	0.97 (233)
HD 93129	0.63 ± 0.03	0.31 ± 0.02	57.17 ± 0.13	2.28 ± 0.08	56.26 ± 0.02	1.30 ± 0.19	0.25 ± 0.03	1.76 (466)
HD 93205	0.30 ± 0.04	0.34 ± 0.03	56.39 ± 0.17	1.71 ± 0.30	55.38 ± 0.11	1.28 ± 0.28	0.54 ± 0.12	1.33 (389)
HD 93250	<0.008	0.74 ± 0.04	55.81 ± 0.08	2.93 ± 0.22	55.77 ± 0.03	3.86 ± 0.67	0.23 ± 0.04	1.21 (298)
HD 93403	0.12 ± 0.02	0.72 ± 0.02	55.11 ± 0.06	1.76 ± 0.13	54.91 ± 0.04	5.79 ± 1.27	0.35 ± 0.04	1.29 (423)
HD 97434	<0.037	0.14 ± 0.05	55.39 ± 0.49	0.63 ± 0.03	54.85 ± 0.13	7.39 ± 3.22	0.40 ± 0.13	0.94 (314)
HD 101205	<0.03	0.70 ± 0.04	55.61 ± 0.07	1.59 ± 0.16	55.33 ± 0.07	3.98 ± 0.73	0.26 ± 0.04	1.29 (369)
HD 143275	0.03 ± 0.01	0.27 ± 0.02	52.54 ± 0.18	0.66 ± 0.04	52.42 ± 0.07	7.94 ± 4.55	1.0	1.52 (213)
HD 144217	<0.0018	0.23 ± 0.01	53.88 ± 0.03	0.80 ± 0.01	53.32 ± 0.02	11.98 ± 3.45	0.21 ± 0.01	1.62 (401)
HD 147932	0.11 ± 0.02	0.96 ± 0.04	53.08 ± 0.08	2.60 ± 0.22	53.08 ± 0.05	5.13 ± 1.47	0.23 ± 0.02	1.29 (317)
HD 148937	<0.004	0.69 ± 0.01	55.76 ± 0.04	2.61 ± 0.09	55.73 ± 0.02	5.59 ± 0.59	0.39 ± 0.04	1.66 (479)
HD 152233	0.29 ± 0.02	0.15 ± 0.01	56.49 ± 0.12	0.57 ± 0.01	55.44 ± 0.04	22.61 ± 9.17	1.0	1.74 (354)
HD 152234	<0.014	0.53 ± 0.09	55.31 ± 0.06	1.03 ± 0.13	54.93 ± 0.22	6.12 ± 0.72	0.29 ± 0.03	1.64 (385)
HD 152249	0.25 ± 0.05	0.40 ± 0.09	55.64 ± 0.24	3.88 ± 0.90	54.37 ± 0.09	0.98 ± 0.30	0.38 ± 0.06	1.34 (404)
HD 157246	0.08 ± 0.05	0.13 ± 0.04	54.27 ± 0.77	0.75 ± 0.04	53.92 ± 0.04	8.26 ± 2.98	0.22 ± 0.04	1.1 (292)
HD 167971	0.032 ± 0.02	0.68 ± 0.03	55.31 ± 0.06	2.01 ± 0.15	54.89 ± 0.05	4.17 ± 0.87	0.49 ± 0.07	1.37 (410)
HD 191612	0.51 ± 0.02	0.27 ± 0.00	56.62 ± 0.10	2.30 ± 0.14	55.53 ± 0.04	2.97 ± 0.82	0.60 ± 0.10	1.97 (459)
HD 200775	0.65 ± 0.05	0.19 ± 0.02	55.75 ± 0.19	1.02 ± 0.08	54.53 ± 0.04	5.79 ± 2.14	1.0	1.32 (316)
HD 215835	0.23 ± 0.12	0.35 ± 0.10	56.21 ± 0.44	0.83 ± 0.07	55.62 ± 0.22	141.9 ± 136.8	0.85 ± 0.46	1.16 (265)
HD 287848†	<0.003	0.81 ± 0.03	52.70 ± 0.04	1.73 ± 0.09	53.02 ± 0.03	36.95 ± 10.13	1.0	1.33 (349)
Tr16-22	0.18 ± 0.12	0.73 ± 0.27	54.65 ± 0.37	2.19 ± 0.31	55.21 ± 0.09	8.86 ± 5.59	0.50 ± 0.21	0.91 (368)

$E(B − V)$ are estimated from the "Stilism" interface[5] (Capitanio et al. 2017).

The data reduction is implemented by SAS 19.0 software following the recommendation of the SAS team[6] and described in Section 2 of the paper by Ryspaeva & Kholtygin (2020). First, we extract light curves with 200 s time binning from the European Photon Imaging Camera (EPIC) images. Visual inspection of light curves of supplemented objects does not show fast changes of count rate during the observations. We extract and analyze low-resolution stellar spectra in the 0.2–8 keV energy band from EPIC images.

3. Spectral Fits

We fit stellar spectra by different models in the "XSPEC 12.10.0" package.[7] The EPIC-PN, EPIC-MOS1 and EPIC-MOS2 spectra are fitted simultaneously. We apply the models
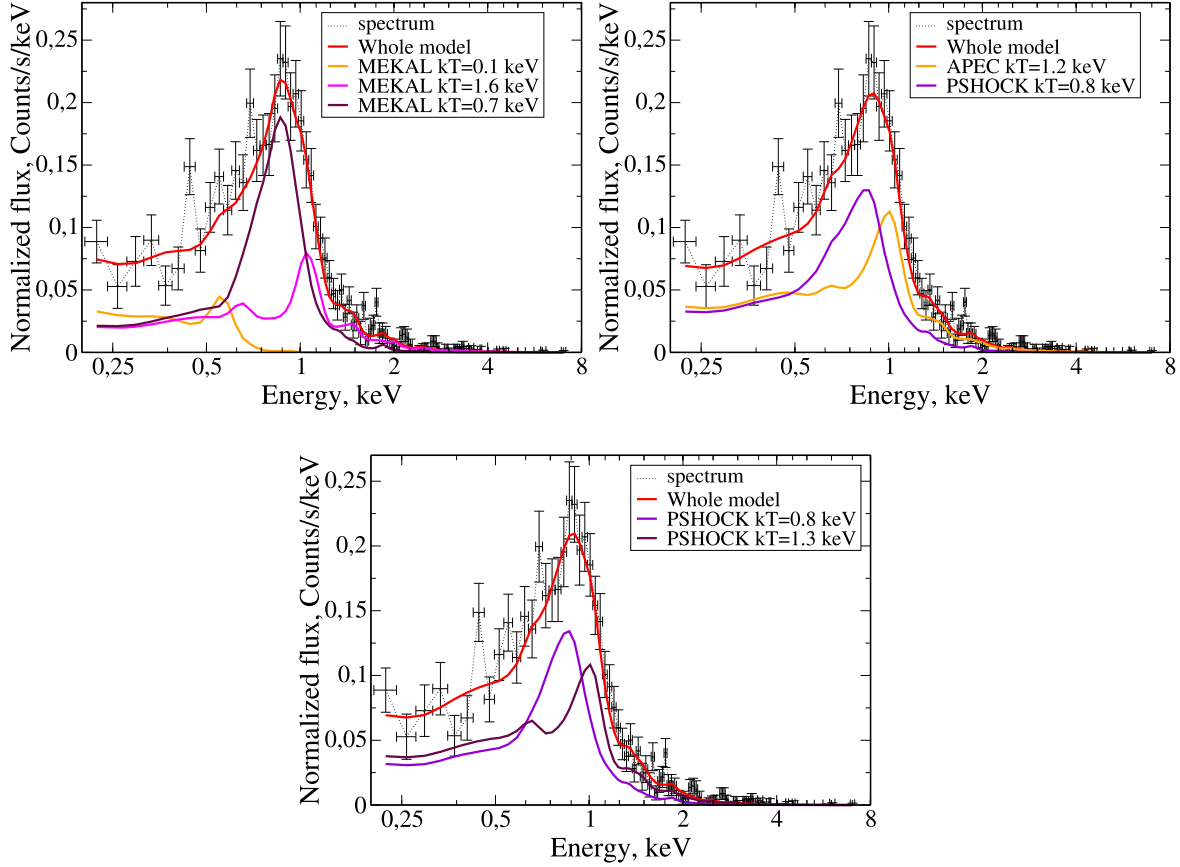

Figure 1. The best fits of the HD 18552 spectrum by different models. The contributions of individual components into the total model X-ray spectrum are shown by colored lines.

Astrophysical Plasma Emission Code (APEC, by Smith et al. 2001), MEKAL (Mewe-Gronenschild-Kaastra by Mewe et al. 1985, 1986; Liedahl et al. 1995)[8] and PSHOCK (by Borkowski et al. 2001). The last one is a model of a plane-parallel postshock wave. The PSHOCK model describes the nonstationary thermal X-ray emission from hot plasma heated by shock waves and characterized by the same parameters as in the APEC and MEKAL models but with an additional ionization timescale parameter τ_u in units of s cm^{-3}

$$\tau_u = T_{\mathrm{char}} \cdot n_{\mathrm{e}}, \tag{1}$$

where n_{e} is the postshock electron number density and T_{char} is the characteristic time. In the original model, PSHOCK was developed for supernova remnants, with T_{char} being the remnant's age t_0. The estimations of this value for the stellar winds are given below (see Section 4 and Equation (6)).

The three above-mentioned models also have a parameter describing metallicity: Abundance. This parameter is defined in terms of solar abundance units according to Anders &

Grevesse (1989). We either use a fixed value of Abundance = 1.0 or find it from the fit of the spectra.

The following model combinations are used:
(1) APEC+APEC, MEKAL+MEKAL
(2) APEC+PSHOCK, APEC+APEC+PSHOCK, MEKAL+PSHOCK, MEKAL+MEKAL+PSHOCK
(3) PSHOCK+PSHOCK

The first group of models describes the stationary thermal emission and is applicable for the MCWS model. The second can describe the X-ray emission containing both stationary and nonstationary components, as in a "hybrid" model by Cassinelly et al., or X-rays from stars with weak magnetic fields when MCWS plays the secondary role. The third group can be useful if the contribution of the nonstationary X-ray emission is dominant.

For all above mentioned sums of models, we estimate average plasma temperature

$$\langle kT \rangle = \frac{\sum_i^N T_i \cdot \mathrm{norm}_i}{\sum_i^N \mathrm{norm}_i}, \tag{2}$$

---

[8] Thereafter—thermal models.

Table 5
The List of X-ray Luminosities and Hardness Ratios Corrected for the Interstellar and Circumstellar Stellar Spectra, Calculated by N_H from APEC/MEKAL Fitting

Star	L_X(0.2-8 keV) 10^{32} erg s^{-1}	HR rel. un.	Star	L_X(0.2-8 keV) 10^{32} erg s^{-1}	HR rel. un.
BD-145040	3.48 ± 2.05	0.13 ± 0.10	HD 120324	$(1.49 \pm 2.80) \cdot 10^{-3}$	0.21 ± 0.05
BD-60501	1.56 ± 0.74	0.20 ± 0.13	HD 127381	$(7.59 \pm 6.19) \cdot 10^{-3}$	0.31 ± 0.28
CPD-282561	11.94 ± 6.70	0.64 ± 0.43	HD 136504	$(2.90 \pm 2.94) \cdot 10^{-3}$	0.60 ± 0.10
HD 101205	22.55 ± 9.93	0.07 ± 0.03	HD 143275	$(5.52 \pm 2.24) \cdot 10^{-2}$	0.02 ± 0.02
HD 108	32.54 ± 8.58	0.22 ± 0.08	HD 144217	$(7.37 \pm 1.90) \cdot 10^{-2}$	0.07 ± 0.02
HD 148937	10.81 ± 2.05	0.64 ± 0.20	HD 147932	$(4.95 \pm 5.05) \cdot 10^{-3}$	0.34 ± 0.04
HD 14947	20.87 ± 17.28	0.20 ± 0.15	HD 152234	10.66 ± 4.70	0.05 ± 0.04
HD 152233	17.15 ± 7.83	0.03 ± 0.02	HD 157246	0.17 ± 0.03	0.09 ± 0.03
HD 152248	22.90 ± 9.37	0.05 ± 0.03	HD 182180	$(2.74 \pm 1.42) \cdot 10^{-2}$	1.27 ± 0.97
HD 152249	6.42 ± 3.56	0.19 ± 0.18	HD 18552	$(3.82 \pm 9.78) \cdot 10^{-3}$	0.35 ± 0.18
HD 152408	4.77 ± 3.53	0.17 ± 0.14	HD 193924	$(6.54 \pm 2.36) \cdot 10^{-4}$	0.18 ± 0.06
HD 15558	18.32 ± 7.15	0.07 ± 0.03	HD 200775	1.07 ± 0.13	0.09 ± 0.01
HD 15570	10.66 ± 6.03	0.08 ± 0.05	HD 21856	$(5.17 \pm 3.35) \cdot 10^{-2}$	0.22 ± 0.15
HD 155806	1.82 ± 0.41	0.04 ± 0.02	HD 219688	$(6.46 \pm 2.71) \cdot 10^{-3}$	0.46 ± 0.24
HD 15629	7.77 ± 5.22	0.04 ± 0.02	HD 24398	0.16 ± 0.05	0.06 ± 0.03
HD 159176	6.32 ± 1.74	0.06 ± 0.02	HD 24760	0.10 ± 0.03	0.04 ± 0.02
HD 164794	16.54 ± 3.22	0.08 ± 0.03	HD 261938	0.18 ± 0.08	0.26 ± 0.15
HD 16691	3.79 ± 2.43	0.27 ± 0.19	HD 287848	$(5.97 \pm 1.03) \cdot 10^{-2}$	0.24 ± 0.04
HD 167971	3.88 ± 0.92	0.17 ± 0.05	HD 287849	$(3.66 \pm 1.19) \cdot 10^{-2}$	0.37 ± 0.16
HD 188001	12.15 ± 5.37	0.04 ± 0.02	HD 33328	$(2.11 \pm 9.88) \cdot 10^{-3}$	0.76 ± 0.50
HD 191612	13.24 ± 5.25	0.27 ± 0.15	HD 3360	$(1.58 \pm 7.39) \cdot 10^{-3}$	0.66 ± 0.51
HD 210839	4.11 ± 2.49	0.06 ± 0.04	HD 33904	$(6.85 \pm 6.78) \cdot 10^{-4}$	0.14 ± 0.01
HD 215835	51.84 ± 28.62	0.04 ± 0.03	HD 34816	$(9.12 \pm 2.63) \cdot 10^{-2}$	0.06 ± 0.03
HD 34078	0.69 ± 0.24	0.02 ± 0.01	HD 35468	$(3.30 \pm 1.01) \cdot 10^{-3}$	0.10 ± 0.04
HD 36512	0.53 ± 0.09	0.05 ± 0.01	HD 36959	$(8.68 \pm 1.74) \cdot 10^{-2}$	0.26 ± 0.04
HD 47129	3.50 ± 0.35	0.24 ± 0.02	HD 36960	0.51 ± 0.05	0.20 ± 0.02
HD 47839	0.25 ± 0.04	0.018 ± 0.00	HD 37000	0.16 ± 0.04	0.14 ± 0.07
HD 54662	3.86 ± 1.18	0.04 ± 0.02	HD 37025	$(2.62 \pm 1.04) \cdot 10^{-2}$	0.56 ± 0.26
HD 54879	1.83 ± 0.75	0.14 ± 0.09	HD 37479	0.53 ± 0.05	0.51 ± 0.06
HD 57682	3.59 ± 1.56	0.32 ± 0.15	HD 46328	0.40 ± 0.06	0.05 ± 0.01
HD 93129	45.18 ± 12.22	0.23 ± 0.05	HD 43285	$(1.51 \pm 6.55) \cdot 10^{-3}$	0.23 ± 0.13
HD 93205	49.40 ± 16.20	0.06 ± 0.02	HD 50707	$(6.59 \pm 3.19) \cdot 10^{-2}$	0.34 ± 0.27
HD 93403	3.80 ± 1.57	0.17 ± 0.08	HD 63425	0.47 ± 0.20	0.29 ± 0.12
HD 93521	1.74 ± 1.02	0.26 ± 0.17	HD 63922	0.54 ± 0.14	0.05 ± 0.02
HD 97434	5.22 ± 2.38	0.09 ± 0.04	HD 64760	0.79 ± 0.13	0.16 ± 0.03
HD 17505	2.23 ± 0.90	0.29 ± 0.13	HD 66665	0.27 ± 0.11	0.41 ± 0.27
Tr16-22	12.53 ± 9.07	0.27 ± 0.21	HD 79351	$(3.20 \pm 1.13) \cdot 10^{-3}$	0.19 ± 0.02
BD+433654	4.48 ± 2.21	0.11 ± 0.06	HD 83953	$(2.60 \pm 4.75) \cdot 10^{-3}$	0.55 ± 0.22
ALS18058	$(5.68 \pm 2.17) \cdot 10^{-2}$	0.14 ± 0.06	HD 93250	29.65 ± 10.13	0.24 ± 0.10
BD-124982	3.18 ± 2.16	0.32 ± 0.27	HD 93128	41.15 ± 22.97	0.10 ± 0.04
HD 101444	$(2.82 \pm 1.00) \cdot 10^{-3}$	0.16 ± 0.09	HD 165024	$(3.85 \pm 8.54) \cdot 10^{-3}$	0.09 ± 0.02
HD 105382	$(2.68 \pm 1.19) \cdot 10^{-3}$	0.23 ± 0.13			

where T_i is the temperature of the plasma component with a number i in keV, norm$_i$ is the corresponding normalization parameter and N is the number of components.

For taking into account the interstellar absorption and possible circumstellar absorption of X-rays, the sums of additive models APEC, MEKAL or PSHOCK are multiplied in the model The Tuebingen-Boulder ISM absorption (TBABS) by Wilms et al. (2000). This model presents the cross section for X-ray absorption in the interstellar medium (ISM) as a sum of the cross sections for absorption by the gas-phase ISM, the grain-phase ISM and the molecules in the ISM.

TBABS is characterized by a single parameter of hydrogen column density in the direction to the object N_H (in units of 10^{22} cm^{-2}). To estimate a possible local X-ray absorption by gas and dust in the stellar winds and/or circumstellar disks, we subtract the interstellar values from N_H values obtained by us. Those are calculated following Gudennavar et al. (2012) as

$$N_H^{ISM} = E(B - V) \cdot 6.12 \cdot 10^{21} \text{ cm}^2. \qquad (3)$$

In case the total hydrogen column density N_H from our model fit appears to be less then interstellar value N_H^{ISM}, we fix the N_H value estimated by Equation (3) in the TBABS model

Table 6
The List of X-ray Luminosities and Hardness Ratios of Unabsorbed Stellar Spectra, Calculated by N_{H} from APEC/MEKAL+PSHOCK and PSHOCK+PSHOCK Fitting

Star	APEC/MEKAL+PSHOCK		PSHOCK+PSHOCK	
	L_{X}(0.2–8 keV), 10^{32} erg s^{-1}	HR. rel. un.	L_{X}(0.2–8 keV), 10^{32} erg s^{-1}	HR. rel. un.
ALS18058	$(6.14 \pm 2.91) \cdot 10^{-2}$	0.14 ± 0.07	$(3.47 \pm 9.60) \cdot 10^{-3}$	0.22 ± 0.07
BD+433654	3.77 ± 0.94	0.12 ± 0.04	4.01 ± 2.09	0.13 ± 0.08
BD-145040	4.74 ± 1.76	0.06 ± 0.04	$\cdots$	$\cdots$
CPD-282561	21.07 ± 15.46	0.50 ± 0.40	49.32 ± 44.09	0.66 ± 0.62
HD 101205	24.88 ± 9.66	0.06 ± 0.02	11.56 ± 1.72	0.11 ± 0.02
HD 10144	$(2.63 \pm 3.67) \cdot 10^{-4}$	0.16 ± 0.08	$(2.14 \pm 8.41) \cdot 10^{-4}$	0.24 ± 0.14
HD 108	26.98 ± 5.62	0.28 ± 0.07	70.16 ± 17.92	0.10 ± 0.03
HD 120324	$(1.19 \pm 1.14) \cdot 10^{-3}$	0.27 ± 0.04	$\cdots$	$\cdots$
HD 143275	$\cdots$	$\cdots$	$(2.96 \pm 6.59) \cdot 10^{-3}$	0.04 ± 0.02
HD 144217	$(6.12 \pm 8.89) \cdot 10^{-3}$	0.06 ± 0.01	$(4.21 \pm 1.45) \cdot 10^{-3}$	0.12 ± 0.01
HD 147932	$\cdots$	$\cdots$	$(4.81 \pm 5.47) \cdot 10^{-3}$	0.36 ± 0.05
HD 148937	18.98 ± 2.58	0.29 ± 0.06	19.62 ± 2.08	0.26 ± 0.03
HD 152233	15.78 ± 6.26	0.03 ± 0.02	15.70 ± 7.03	0.03 ± 0.02
HD 152234	6.08 ± 1.99	0.07 ± 0.04	5.51 ± 1.89	0.07 ± 0.04
HD 152249	6.56 ± 2.46	0.12 ± 0.10	8.19 ± 3.56	0.11 ± 0.10
HD 15558	10.05 ± 3.19	0.12 ± 0.05	10.27 ± 3.77	0.12 ± 0.05
HD 15570	8.36 ± 2.79	0.07 ± 0.04	11.03 ± 5.98	0.07 ± 0.05
HD 155806	0.47 ± 0.30	0.39 ± 0.32	$\cdots$	$\cdots$
HD 157246	0.39 ± 0.12	0.04 ± 0.02	0.22 ± 0.10	0.08 ± 0.04
HD 159176	6.01 ± 1.63	0.07 ± 0.02	$\cdots$	$\cdots$
HD 167971	3.95 ± 0.99	0.15 ± 0.03	3.94 ± 0.97	0.15 ± 0.03
HD 17505	2.51 ± 0.68	0.21 ± 0.06	2.51 ± 0.68	0.21 ± 0.06
HD 18552	$(3.32 \pm 4.71) \cdot 10^{-3}$	0.37 ± 0.16	$(3.38 \pm 5.38) \cdot 10^{-3}$	0.37 ± 0.16
HD 191612	12.14 ± 3.74	0.28 ± 0.12	24.51 ± 9.77	0.14 ± 0.08
HD 193924	$(4.64 \pm 8.98) \cdot 10^{-5}$	0.25 ± 0.04	$\cdots$	$\cdots$
HD 200775	$\cdots$	$\cdots$	0.97 ± 0.24	0.10 ± 0.03
HD 215835	39.31 ± 23.45	0.06 ± 0.04	40.07 ± 24.46	0.06 ± 0.04
HD 24398	0.17 ± 0.06	0.06 ± 0.02	0.16 ± 0.06	0.07 ± 0.03
HD 24760	$(9.97 \pm 4.89) \cdot 10^{-2}$	0.05 ± 0.03	$\cdots$	$\cdots$
HD 287848	$(4.88 \pm 2.10) \cdot 10^{-3}$	0.26 ± 0.02	$(4.89 \pm 2.14) \cdot 10^{-3}$	0.29 ± 0.02
HD 287849	$(3.03 \pm 5.69) \cdot 10^{-3}$	0.36 ± 0.03	$\cdots$	$\cdots$
HD 36512	$\cdots$	$\cdots$	0.55 ± 0.10	0.04 ± 0.01
HD 33904	$(7.24 \pm 6.97) \cdot 10^{-4}$	0.14 ± 0.02	$\cdots$	$\cdots$
HD 34078	0.79 ± 0.31	0.02 ± 0.01	$\cdots$	$\cdots$
HD 37000	$\cdots$	$\cdots$	0.33 ± 0.13	0.06 ± 0.01
HD 37479	0.46 ± 0.04	0.58 ± 0.06	$\cdots$	$\cdots$
HD 46328	$\cdots$	$\cdots$	0.37 ± 0.06	0.05 ± 0.01
HD 47129	4.00 ± 0.76	0.22 ± 0.06	3.58 ± 0.50	0.26 ± 0.06
HD 47839	0.26 ± 0.023	0.015 ± 0.002	$\cdots$	$\cdots$
HD 54662	4.14 ± 2.03	0.04 ± 0.02	3.59 ± 1.71	0.04 ± 0.02
HD 54879	1.40 ± 0.50	0.16 ± 0.08	1.43 ± 0.53	0.16 ± 0.08
HD 57682	2.73 ± 0.50	0.32 ± 0.17	2.64 ± 0.42	0.32 ± 0.16
HD 63922	0.49 ± 0.12	0.05 ± 0.02	0.55 ± 0.16	0.05 ± 0.02
HD 64760	0.80 ± 0.15	0.15 ± 0.02	0.67 ± 0.11	0.20 ± 0.04
HD 79351	$\cdots$	$\cdots$	$(3.19 \pm 1.22) \cdot 10^{-3}$	0.19 ± 0.02
HD 83953	$(2.15 \pm 2.35) \cdot 10^{-3}$	0.66 ± 0.11	$(2.16 \pm 2.38) \cdot 10^{-3}$	0.66 ± 0.11
HD 93128	13.80 ± 4.26	0.27 ± 0.10	16.88 ± 6.65	0.24 ± 0.10
HD 93129	52.42 ± 12.51	0.18 ± 0.07	47.81 ± 12.79	0.23 ± 0.06
HD 93205	18.77 ± 7.52	0.10 ± 0.03	41.91 ± 13.33	0.05 ± 0.03
HD 93250	28.74 ± 13.75	0.32 ± 0.19	22.73 ± 1.81	0.27 ± 0.05
HD 93403	3.38 ± 0.68	0.16 ± 0.07	3.48 ± 0.72	0.16 ± 0.07
HD 93521	1.73 ± 0.81	0.19 ± 0.09	$\cdots$	$\cdots$
HD 97434	5.52 ± 2.95	0.10 ± 0.06	4.48 ± 2.11	0.12 ± 0.05
Tr16-22	10.80 ± 6.63	0.25 ± 0.18	10.20 ± 5.86	0.24 ± 0.16

Table 7
Parameters of Best Dependences between Unabsorbed X-ray Luminosity and Stellar Characteristics

Approximation	Stars	Fit	R	N	FAP	α	β
All examined stars							
$L_X(0.2\text{–}8\ \text{keV}) = \alpha \cdot \eta^{\beta}$	OB	A	-0.63 ± 0.00	16	0.008	$(1.78 \pm 0.69) \cdot 10^{33}$	-0.47 ± 0.03
		AS	-0.80 ± 0.02	9	0.013	$(3.05 \pm 0.13) \cdot 10^{33}$	-0.32 ± 0.03
		2S	-0.76 ± 0.05	10	0.020	$(1.32 \pm 0.69) \cdot 10^{34}$	-0.66 ± 0.06
$L_X(0.2\text{–}8\ \text{keV}) = \alpha \cdot E_{\text{kin}}^{\beta}$	OB	A	0.82 ± 0.01	47	0.001	$(2.42 \pm 0.37) \cdot 10^{11}$	0.56 ± 0.01
		AS	0.76 ± 0.01	27	0.001	$(6.32 \pm 0.31) \cdot 10^{13}$	0.52 ± 0.02
		2S	0.69 ± 0.01	25	0.000	$(2.63 \pm 0.84) \cdot 10^{14}$	0.48 ± 0.02
	O	A	0.55 ± 0.03	30	0.004	$(1.95 \pm 0.16) \cdot 10^{25}$	0.21 ± 0.02
		AS	0.60 ± 0.03	21	0.007	$(1.78 \pm 0.12) \cdot 10^{25}$	0.21 ± 0.01
		2S	0.63 ± 0.01	19	0.005	$(7.80 \pm 2.57) \cdot 10^{23}$	0.25 ± 0.01
	B	A	0.83 ± 0.00	17	0.001	$(1.38 \pm 0.99) \cdot 10^{9}$	0.61 ± 0.01
$L_X(0.2\text{–}8\ \text{keV}) = \alpha \cdot F_{\text{M}}^{\beta}$	OB	A	0.78 ± 0.01	45	<0.001	$(2.61 \pm 0.76) \cdot 10^{17}$	0.54 ± 0.02
		2S	0.69 ± 0.01	23	<0.001	$(9.55 \pm 3.05) \cdot 10^{18}$	0.50 ± 0.02
		AS	0.75 ± 0.01	26	<0.001	$(1.65 \pm 0.81) \cdot 10^{18}$	0.52 ± 0.02
	O	A	0.53 ± 0.04	30	0.007	$(8.16 \pm 6.20) \cdot 10^{26}$	0.22 ± 0.03
		2S	0.63 ± 0.01	19	0.005	$(3.56 \pm 1.07) \cdot 10^{25}$	0.27 ± 0.01
		AS	0.59 ± 0.03	21	0.008	$(4.22 \pm 2.72) \cdot 10^{26}$	0.23 ± 0.01
	B	A	0.64 ± 0.02	15	0.014	$(1.65 \pm 0.83) \cdot 10^{18}$	0.49 ± 0.04
Magnetic stars							
$L_X(0.2\text{–}8\ \text{keV}) = \alpha \cdot E_{\text{kin}}^{\beta}$	OB	A	0.788 ± 0.001	23	0.001	$(9.08 \pm 5.85) \cdot 10^{12}$	0.54 ± 0.01
	B	A	0.82 ± 0.03	10	0.006	$(8.43 \pm 7.46) \cdot 10^{19}$	0.66 ± 0.04
$L_X(0.2\text{–}8\ \text{keV}) = \alpha \cdot F_{\text{M}}^{\beta}$	OB	A	0.72 ± 0.02	23	<0.001	$(1.28 \pm 0.35) \cdot 10^{18}$	0.48 ± 0.02
		AS	0.594 ± 0.004	12	0.04	$(1.81 \pm 1.63) \cdot 10^{23}$	0.36 ± 0.04
Nonmagnetic stars							
$L_X(0.2\text{–}8\ \text{keV}) = \alpha \cdot E_{\text{kin}}^{\beta}$	OB	A	0.84 ± 0.01	24	0.001	$(2.45 \pm 1.58) \cdot 10^{19}$	0.58 ± 0.02
		AS	0.85 ± 0.01	16	0.001	$(7.15 \pm 2.97) \cdot 10^{19}$	0.60 ± 0.02
		2S	0.87 ± 0.01	15	0.001	$(5.42 \pm 4.07) \cdot 10^{19}$	0.68 ± 0.02
	O	A	0.70 ± 0.06	17	0.005	$(2.15 \pm 2.08) \cdot 10^{19}$	0.28 ± 0.03
		AS	0.85 ± 0.03	11	0.002	$(9.75 \pm 8.87) \cdot 10^{19}$	0.26 ± 0.01
		2S	0.80 ± 0.01	10	0.006	$(1.80 \pm 1.62) \cdot 10^{19}$	0.38 ± 0.02
$L_X(0.2\text{–}8\ \text{keV}) = \alpha \cdot F_{\text{M}}^{\beta}$	OB	A	0.84 ± 0.01	22	<0.001	$(1.77 \pm 1.02) \cdot 10^{15}$	0.62 ± 0.02
		2S	0.84 ± 0.01	13	<0.001	$(2.09 \pm 1.55) \cdot 10^{13}$	0.69 ± 0.02
		AS	0.85 ± 0.01	14	<0.001	$(5.91 \pm 1.97) \cdot 10^{14}$	0.64 ± 0.02
	O	A	0.68 ± 0.06	17	0.007	$(1.34 \pm 1.26) \cdot 10^{25}$	0.29 ± 0.04
		2S	0.78 ± 0.01	10	0.009	$(2.05 \pm 1.72) \cdot 10^{22}$	0.39 ± 0.02
		AS	0.84 ± 0.03	11	0.003	$(3.32 \pm 2.97) \cdot 10^{25}$	0.28 ± 0.02

Designations: A—APEC/MEKAL, AS—APEC/MEKAL+PSHOCK, 2S—PSHOCK+PSHOCK.

Note. The proposed approximations are listed in the 1st column. The 2nd column contains the sample of stars. Spectral models are indicated in the 3rd column. The 4th column includes the correlation coefficients. Numbers of points and upper limits for False Alarm Probability (FAP) are written in the 5th and 6th columns respectively. Coefficients of approximations are given in the 7th and 8th columns.

and multiply the sum of models by the additional model Photoelectric Absorption (PHABS) by Balucinska-Church & McCammon (1992) to determine the local $N_{\text{H}}^{\text{local}}$. The results of our best spectral fits are presented in Tables 2, 3 and 4. Figure 1 demonstrates the examples of model spectral fits with the component resolution for HD 18552.

We calculate the corrected by ISM and circumstellar absorption fluxes in stellar spectra according to approximation formulas by Morrison & McCammon (1983) by using the total N_{H} value from our spectral fits. We also estimated two characteristics of the spectra, corrected for the ISM and/or

circumstellar absorption: X-ray luminosity in an energy interval 0.2–8 keV

$$L_X = 4\pi d^2 H(0.2\text{–}8\ \text{keV}), \quad [\text{erg s}^{-1}], \qquad (4)$$

where d is the distance to the star and $H(0.2\text{–}8\ \text{keV})$ is the X-ray flux in an energy band 0.2–8 keV; and a hardness ratio (i.e., Nazé et al. 2014)

$$\text{HR} = \frac{H(2\text{–}8\ \text{keV})}{H(0.2\text{–}2\ \text{keV})}. \qquad (5)$$

The lists of these values are given in Tables 5 and 6.

Table 8
The Same as in Table 7, But for Dependences between Plasma Temperatures and Stellar Parameters

Approximation	Stars	Spectral Fits	R	N	FAP	α	β
All examined stars							
$\langle kT \rangle = \alpha \cdot HR^{\beta}$	OB	A	0.62 ± 0.11	79	0.001	1.29 ± 0.62	0.52 ± 0.05
		AS	0.57 ± 0.15	46	0.004	2.29 ± 1.22	0.59 ± 0.16
		2S	0.58 ± 0.08	41	0.001	1.84 ± 0.68	0.54 ± 0.12
	O	A	0.60 ± 0.18	39	0.007	1.19 ± 0.53	0.53 ± 0.09
		AS	0.53 ± 0.13	29	0.031	2.30 ± 1.38	0.51 ± 0.09
		2S	0.54 ± 0.10	24	0.034	1.95 ± 0.73	0.52 ± 0.18
	B	A	0.61 ± 0.15	40	0.003	1.46 ± 0.83	0.47 ± 0.13
$\langle kT \rangle = \alpha + HR \cdot \beta$	B	AS	0.71 ± 0.10	17	0.009	0.16 ± 0.50	5.13 ± 2.90
		2S	0.78 ± 0.07	17	0.001	0.21 ± 0.19	3.50 ± 1.78
$\langle kT \rangle = \alpha + v_{\infty} \cdot \beta$	OB	2S	0.42 ± 0.05	29	0.046	-0.011 ± 0.014	$(2.91 \pm 0.86) \cdot 10^{-5}$
$\langle kT \rangle = \alpha \cdot \dot{M}^{\beta}$	OB	2S	0.45 ± 0.06	26	0.045	3.74 ± 1.05	0.134 ± 0.008
$\langle kT \rangle = \alpha \cdot E_{\text{kin}}^{\beta}$	OB	2S	0.48 ± 0.09	26	0.047	$(1.66 \pm 1.06) \cdot 10^{-5}$	0.125 ± 0.012
$kT_{\text{pshock}} = \alpha \cdot HR^{\beta}$	OB	AS	0.40 ± 0.05	46	0.016	2.72 ± 1.08	0.40 ± 0.05
	O	AS	0.45 ± 0.05	29	0.033	2.99 ± 1.27	0.40 ± 0.06
$kT_{\text{pshock}} = \alpha \cdot \dot{M}^{\beta}$	OB	AS	0.63 ± 0.11	28	0.005	9.55 ± 2.78	0.14 ± 0.03
$kT_{\text{pshock}} = \alpha \cdot E_{\text{kin}}^{\beta}$	OB	AS	0.65 ± 0.10	28	0.025	$(2.91 \pm 2.87) \cdot 10^{-4}$	0.12 ± 0.03
$kT_{\text{pshock}} = \alpha \cdot F_{\text{M}}^{\beta}$	OB	AS	0.48 ± 0.10	27	0.047	$(9.43 \pm 9.01) \cdot 10^{-3}$	0.10 ± 0.03
	O	AS	0.57 ± 0.06	22	0.014	$(4.39 \pm 2.92) \cdot 10^{-4}$	0.13 ± 0.01
$kT_{\text{apec}} = \alpha \cdot HR^{\beta}$	OB	AS	0.47 ± 0.07	46	0.005	1.24 ± 0.32	0.44 ± 0.09
	O	AS	0.45 ± 0.06	29	0.040	1.50 ± 0.65	0.41 ± 0.06
Magnetic stars							
$\langle kT \rangle = \alpha \cdot HR^{\beta}$	OB	A	0.69 ± 0.04	29	0.001	1.78 ± 1.04	0.59 ± 0.06
		AS	0.68 ± 0.08	16	0.015	2.81 ± 1.19	0.64 ± 0.18
	O	A	0.79 ± 0.06	17	0.001	2.20 ± 1.11	0.71 ± 0.10
		AS	0.64 ± 0.11	14	0.048	2.69 ± 1.27	0.60 ± 0.17
Nonmagnetic stars							
$\langle kT \rangle = \alpha \cdot HR^{\beta}$	OB	A	0.54 ± 0.16	50	0.007	0.98 ± 0.41	0.44 ± 0.06
		2S	0.59 ± 0.10	28	0.007	2.19 ± 1.03	0.62 ± 0.10
	O	2S	0.67 ± 0.08	13	0.033	3.20 ± 1.83	0.75 ± 0.19
	B	A	0.67 ± 0.11	28	0.002	1.40 ± 0.65	0.52 ± 0.08
$\langle kT \rangle = \alpha + HR \cdot \beta$	B	AS	0.63 ± 0.11	15	0.046	0.26 ± 0.52	4.97 ± 4.01
	B	2S	0.77 ± 0.08	15	0.004	0.23 ± 0.23	3.51 ± 1.81
$kT_{\text{pshock}} = \alpha \cdot F_{\text{M}}^{\beta}$	OB	AS	0.69 ± 0.11	15	0.034	$(1.65 \pm 1.64) \cdot 10^{-3}$	0.14 ± 0.04
	O	AS	0.71 ± 0.03	12	0.016	$(2.80 \pm 2.24) \cdot 10^{-5}$	0.17 ± 0.01
$kT_{\text{apec}} = \alpha \cdot HR^{\beta}$	OB	AS	0.46 ± 0.05	30	0.026	1.10 ± 0.23	0.43 ± 0.11

4. The Dependences Between Parameters of X-ray Spectra

As follows from the previous section, all studied X-ray spectra can be fitted by the multitemperature APEC/MEKAL model, and the X-ray spectra of 56% of examined OB stars (75% of all target O stars and 39% of B stars) can be described by thermal models with an additional PSHOCK component. Moreover, 50% of considered spectra (62.5% of target O stars and 39% of B stars) can be fitted by the model PSHOCK +PSHOCK.

We find that 43% of O stars, whose spectra can be fitted by the APEC/MEKAL+PSHOCK model, are magnetic and 44% of O stars, whose spectra can be fitted by PSHOCK+PSHOCK model, are magnetic. At the same time only 11% of B stars, whose spectra can be fitted by APEC/MEKAL+PSHOCK or

PSHOCK+PSHOCK models, are magnetic (HD 120324, HD 37479 and HD 200775, HD 46328 respectively). There are four Of?p-type stars (Walborn 1972), CPD-282561, HD 108, HD 148937, and HD 191612, and five particle-accelerating colliding-wind binaries (PACWBs, De Becker & Raucq 2013; De Becker et al. 2017), HD 15558, HD 152408, HD 167971, HD 93129 and HD 93250, in our sample. X-ray spectra of these peculiar OB stars excluding HD 152408 can be fitted by both APEC/MEKAL+PSHOCK and PSHOCK+PSHOCK models.

We test the possible dependencies between X-ray luminosities of studied spectra and stellar parameters such as terminal wind velocity v_{∞}, mass loss rate $\dot{M}$, kinetic energy of stellar wind $E_{\text{kin}} = \dot{M} \cdot v_{\infty}^2$, momentum of stellar wind $F_{\text{M}} = \dot{M} \cdot v_{\infty}$, magnetic confinement parameter η (ud-Doula & Owocki 2002), and magnetic field values. We study correlations for all OB
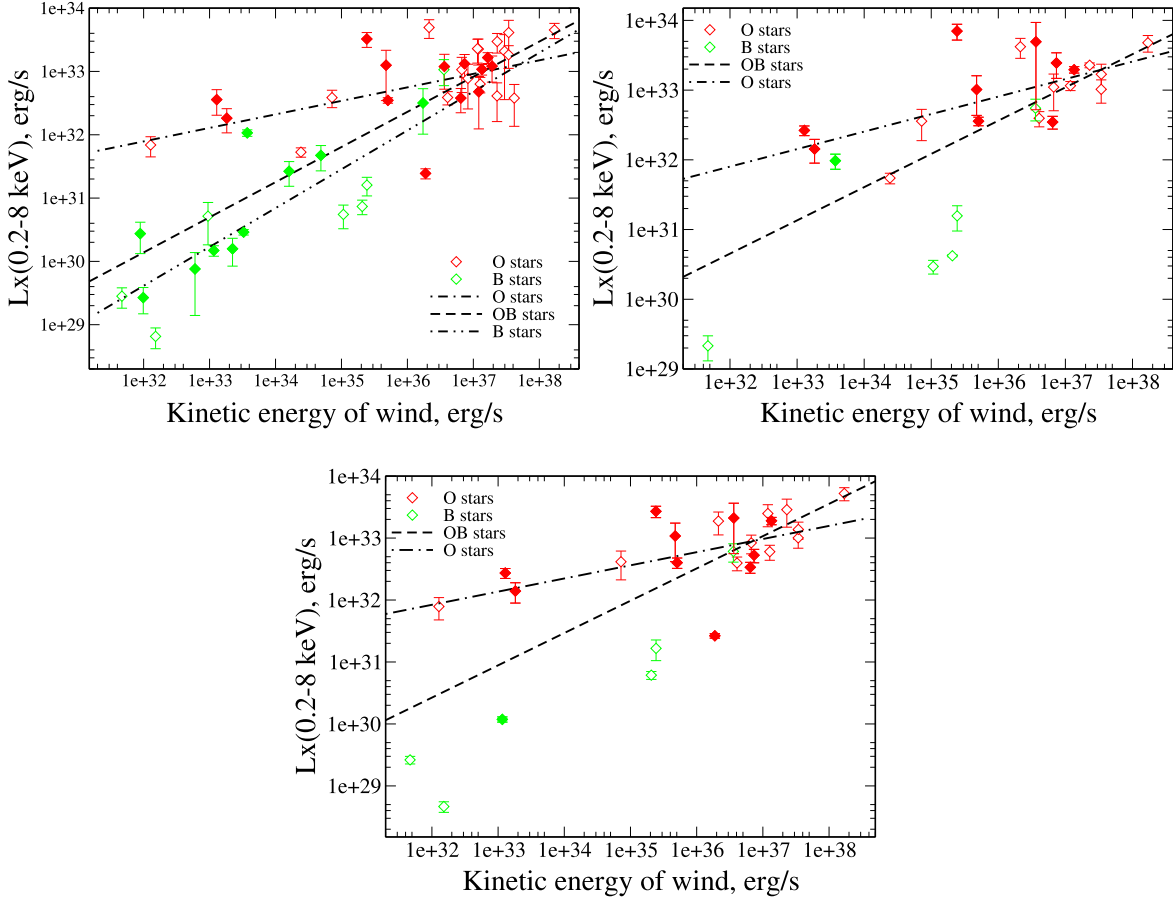
Figure 2. X-ray luminosity vs. kinetic energy of winds for APEC/MEKAL model (top panel, left), PSHOCK+PSHOCK model (top panel, right) and APEC/ MEKAL+PSHOCK model (bottom panel). Fits for OB (dotted lines), O (dash–dotted lines) and B stars (dash-double-dotted lines) are shown. Magnetic and nonmagnetic stars are labeled with filled and empty symbols respectively.

stars from our sample, separately for magnetic and for nonmagnetic stars. Coefficients of the best dependencies are presented in Tables 7 and 8. Figures 2 and 3 demonstrate the selected dependencies.

In addition we study possible correlations between characteristics of model stellar spectra, such as average plasma temperature $\langle kT \rangle$, temperature from PSHOCK component kT_{pshock}, temperature from APEC/MEKAL components kT_{apec}, ionization parameter τ_u, T_{char} and the above characteristics of considered stars. Table 8 gives the approximations of the best dependencies, which are shown in Figures 4–6.

Our regression analysis yields some interesting results. First we confirm a result from our previous paper by Ryspaeva & Kholtygin (2020) about growing X-ray luminosity of OB stars with mass loss rate, kinetic energies of winds and decreasing X-ray luminosity with magnetic confinement parameter, but for a larger sample of objects. Such correlations can be correct for luminosities in the 0.5–8 keV energy band, for which the interstellar absorption of X-rays is not significant. In our

current paper we find similar dependences for X-ray luminosities corrected for absorption in interstellar and circumstellar mediums. Moreover these correlations are valid for spectral fits both by APEC+PSHOCK and PSHOCK+PSHOCK models.

Second, we confirm that in accordance with Ryspaeva & Kholtygin (2020) the plasma temperature from spectral fits by thermal models increases with the hardness ratio for bigger samples of stars. Two similar dependences for average plasma temperature from APEC/MEKAL+PSHOCK and PSHOCK +PSHOCK spectral fits are established. At the same time, we revealed that kT_{pshock} from the APEC/MEKAL+PSHOCK spectral fit increases with F_M and E_{kin} (Figure 5). The $\langle kT \rangle$ from PSHOCK+PSHOCK increases with terminal wind velocity, mass loss rate and E_{kin}, but we do not find any dependencies between this $\langle kT \rangle$ and momentum of stellar wind F_M.

Third, we can note that some dependencies are valid either for both O and B stars, or for O and/or B stars separately. For B-type stars, we yield only two dependencies: L_X versus E_{kin}
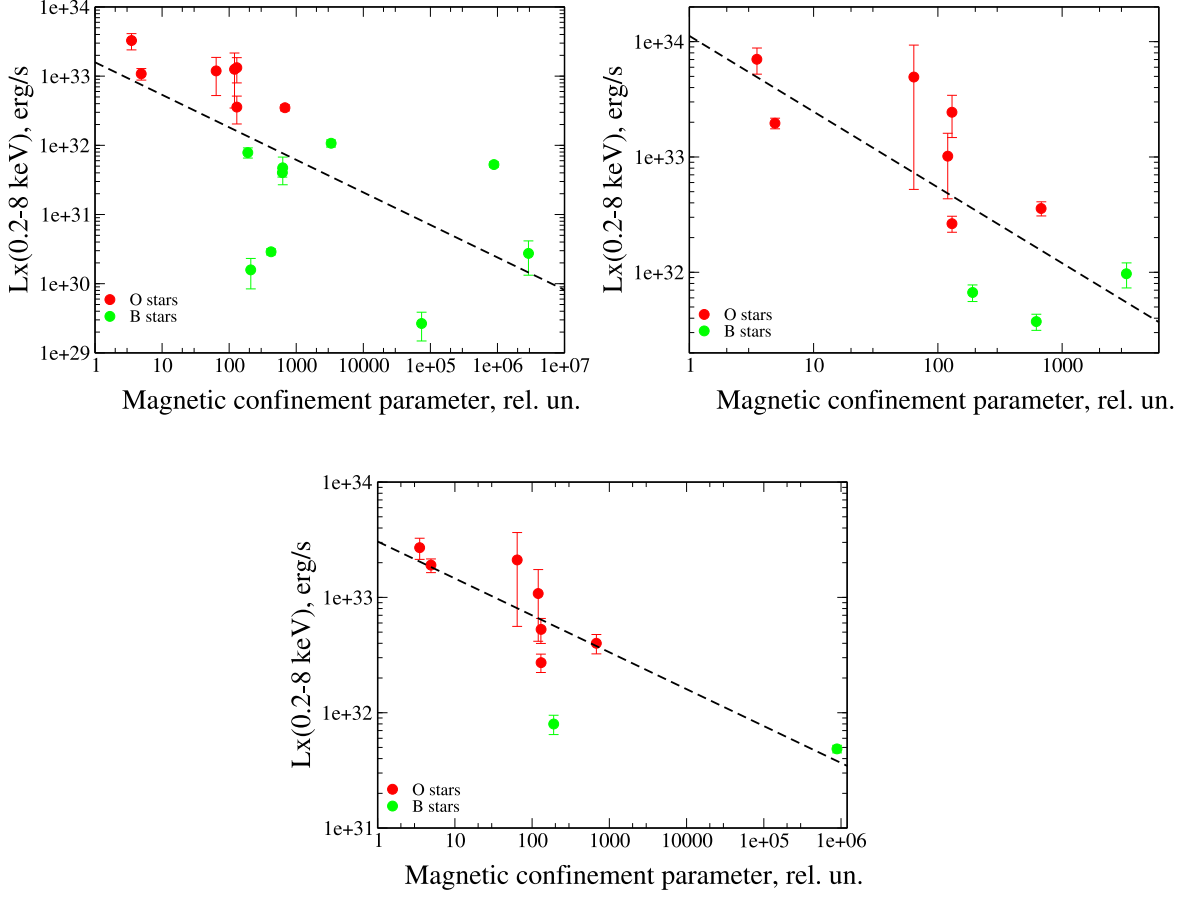
Figure 3. The same as Figure 2 but for the dependences between X-ray luminosity and magnetic confined parameter η. Dashed lines show fits.

and $\langle kT \rangle$ versus *HR*. These correlations occur only in case of spectral fitting by APEC/MEKAL models.

Additionally, we compare $\langle kT \rangle$ from different model spectra. We find the approximal dependence $\langle kT \rangle_{\text{APEC/MEKAL+PSHOCK}} = (0.28 \pm 0.18) + \langle kT \rangle_{\text{APEC/MEKAL}} \cdot (1.36 \pm 0.75)$, $R = 0.70 \pm 0.16$, $N = 46$ and FAP < 0.001, see Figure 8. This correlation is stronger for temperatures from thermal models higher than 0.5 keV.

Herewith, we do not find dependencies between any characteristics of X-ray spectra of studied OB stars and stellar magnetic fields. For example, Figure 7 demonstrates the dependences of three parameters from APEC+PSHOCK spectral fit: hardness ratio, X-ray luminosity and plasma temperature kT_{shock} with magnetic field value. The correlation coefficients of these and other dependences with magnetic fields are rather small. All correlations found in our work hold for spectra of stars with any magnetic field strength. This fact once again confirms the absence of a key role for the stellar magnetic field in the formation of X-rays from OB stars.

The above results allow us to suggest that the PSHOCK model can be useful for describing the X-ray spectra of

OB-type stars, but the question about the interpretation of the ionization parameter τ_u and time T_{char} remains open. We calculate T_{char} using the expression

$$T_{\text{char}} = \frac{\tau_u}{n_e} = \frac{\tau_u}{\sqrt{EM/V_f}}, \qquad (6)$$

where *EM* is emission measure from spectral fit, and V_f is the volume of X-ray emitting plasma. We calculate the volume V_f for each star using the filling factor *f* of the X-ray emitting gas for OB stars, then $V_f = fV$. We fix the volume *V* and use the typical value of $f \sim 0.01$ for all OB stars following Ryspaeva et al. (2023). We calculate time T_{char} using Equation (6), and the results are given in Tables 9, 10.

We trace the possible dependences of this value on the characteristics of stars and their X-ray spectra. The reduction of T_{char} with the kinetic energy and momentum of stellar wind, and decrease of X-ray luminosity with growth of T_{char} are revealed. The last correlation takes place either for the PSHOCK+PSHOCK fit, or for the partially nonstationary X-rays described by APEC+PSHOCK models. Other dependences occur only for the PSHOCK+PSHOCK fit. All these dependences are correct for stars with any strength of magnetic
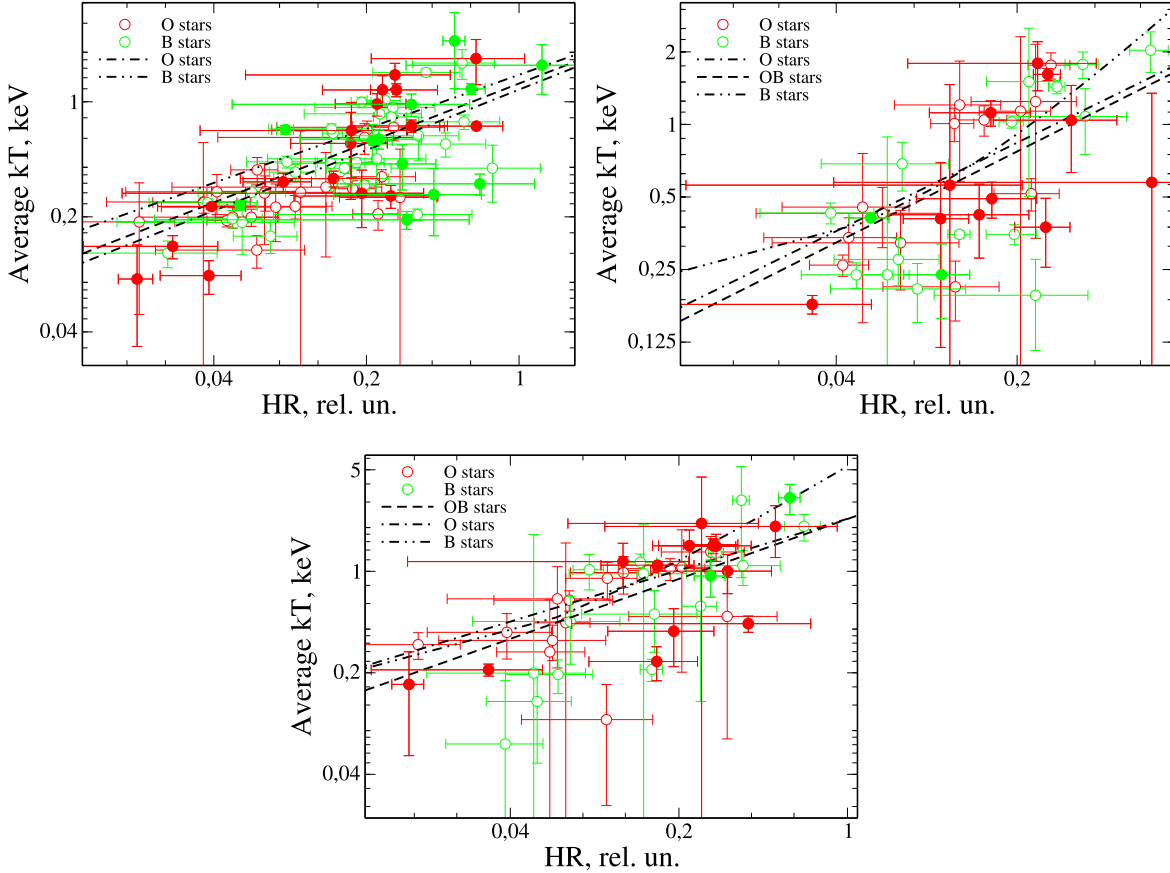
Figure 4. The same as Figure 2 but for dependencies between average plasma temperature and hardness ratio.

field. Figures 9–12 demonstrate these dependences, and approximate parameters are presented in Tables 9–12.

5. Discussion and Conclusion

The results of spectral fitting and regression analysis, presented in the present paper, allow us to infer the next interesting conclusions.

Spectral models with an additional PSHOCK component can describe X-ray spectra of OB stars with any strength of magnetic field and terminal wind velocity. Such modeling for both O and B stars leads to $\tau \sim 10^8 - 10^{13}$ s cm^{-3} and plasma temperature of about 1–5 keV. Average plasma temperature from APEC/MEKAL+PSHOCK modeling is bigger than that from fits with only thermal models for the bulk of studied stars. There is a linear dependence between two such temperatures above 0.5 keV. Model PSHOCK can describe stellar X-ray fluxes generated due to the collision of stellar winds in double and multiple systems.

Moreover, plasma temperature from the PSHOCK model component increases with momentum of stellar wind and kinetic energy of stellar wind by a power law with index

$\sim$0.10–0.14. Ryspaeva & Kholtygin (2020) did not find similar correlations for $\langle kT \rangle$ from spectral fitting by only stationary thermal models. X-ray luminosity of nonstationary X-rays from OB stars increases with momentum and energy of stellar winds by the same power law as for stationary emission (see Nazé et al. 2014; Ryspaeva & Kholtygin 2020).

Herewith, nonstationary stellar X-ray emission is characterized by plasma heating rate, i.e., the T_{char} parameter. This value decreases with energy and momentum of stellar wind by a power law with index $\beta \sim 0.2$–0.3. X-ray luminosity of nonstationary emission decreases with plasma heating rate by a power law with index $\beta \sim -1$. Spectral fits with the PSHOCK component better describe X-ray spectra of O-type stars and all correlations considered by us take place for O-type stars only and differ from those for OB stars (see Tables 10–11). This conclusion can be explained by the faster stellar winds of O-type stars.

In addition we confirm the result from Ryspaeva & Kholtygin (2020) that there is no link between the characteristics of X-rays from OB stars and their magnetic field strength. We do not see significant differences between characteristics of studied X-ray spectra for magnetic and nonmagnetic stars.
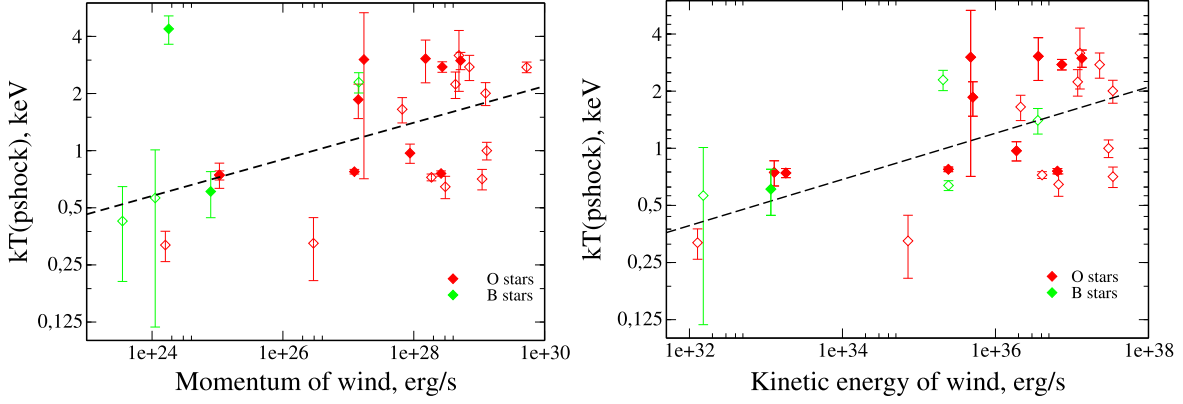
Figure 5. The dependencies of plasma temperature for PSHOCK component on momentum of stellar wind (left panel) and for kinetic energy of wind (right panel), and for APEC/MEKAL+PSHOCK model fits. Linear fits of these dependencies for OB stars are shown by dashed lines. Magnetic and nonmagnetic stars are labeled with filled and empty symbols respectively.
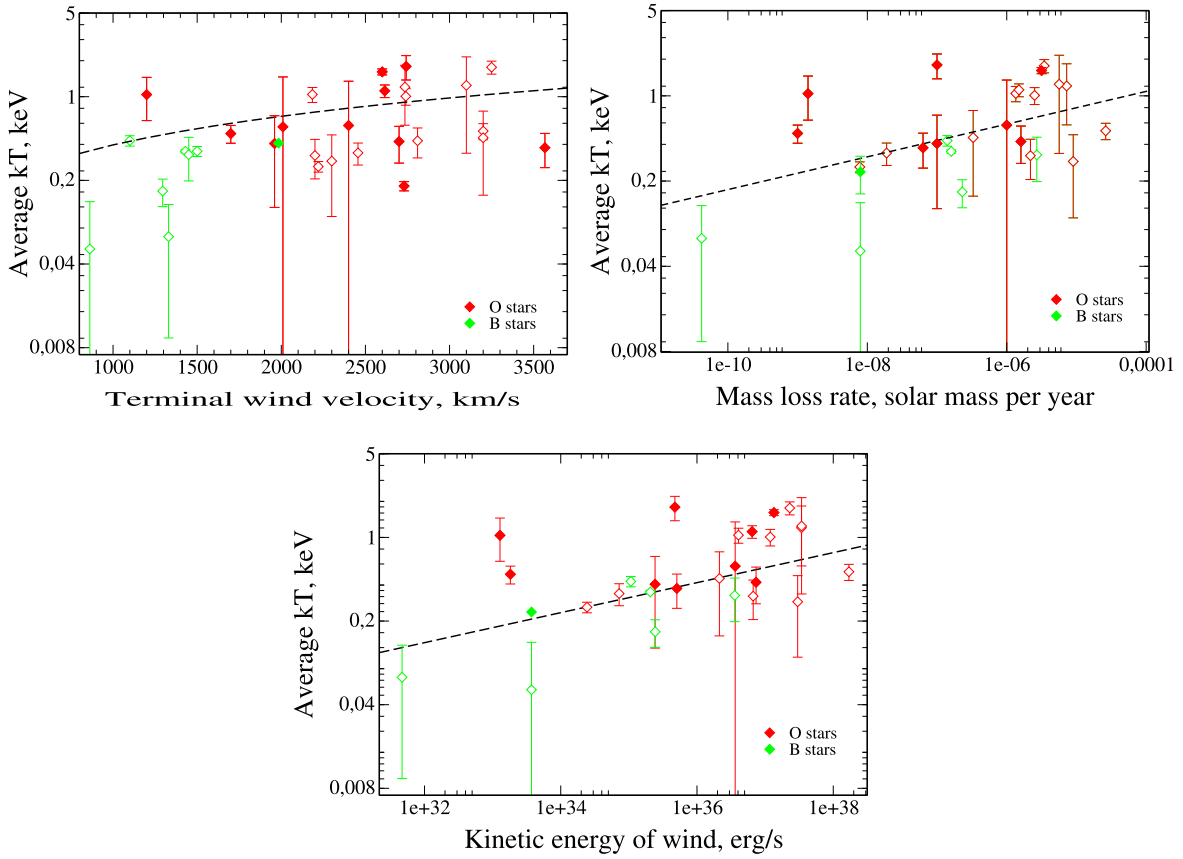

Figure 6. The dependencies between average plasma temperature and terminal wind velocity (top left panel), mass loss rate (top right panel), and kinetic energy of wind (bottom panel) from spectral fits by the PSHOCK+PSHOCK model. Dashed lines show approximations for OB stars. Stars with magnetic fields and nonmagnetic stars are indicated by filled and empty symbols respectively.

We can conclude that the PSHOCK model allows us to check the formation of X-rays in the inhomogeneous stellar winds of OB stars, when shock waves play a key role. Such X-rays should be nonstationary and be described by the PSHOCK model. The value of T_{char} can be specified as the plasma ionization time or the time interval between two shocks in the stellar wind. In a framework of hypotheses about X-rays from inhomogeneous stellar winds, T_{char} can be a time for
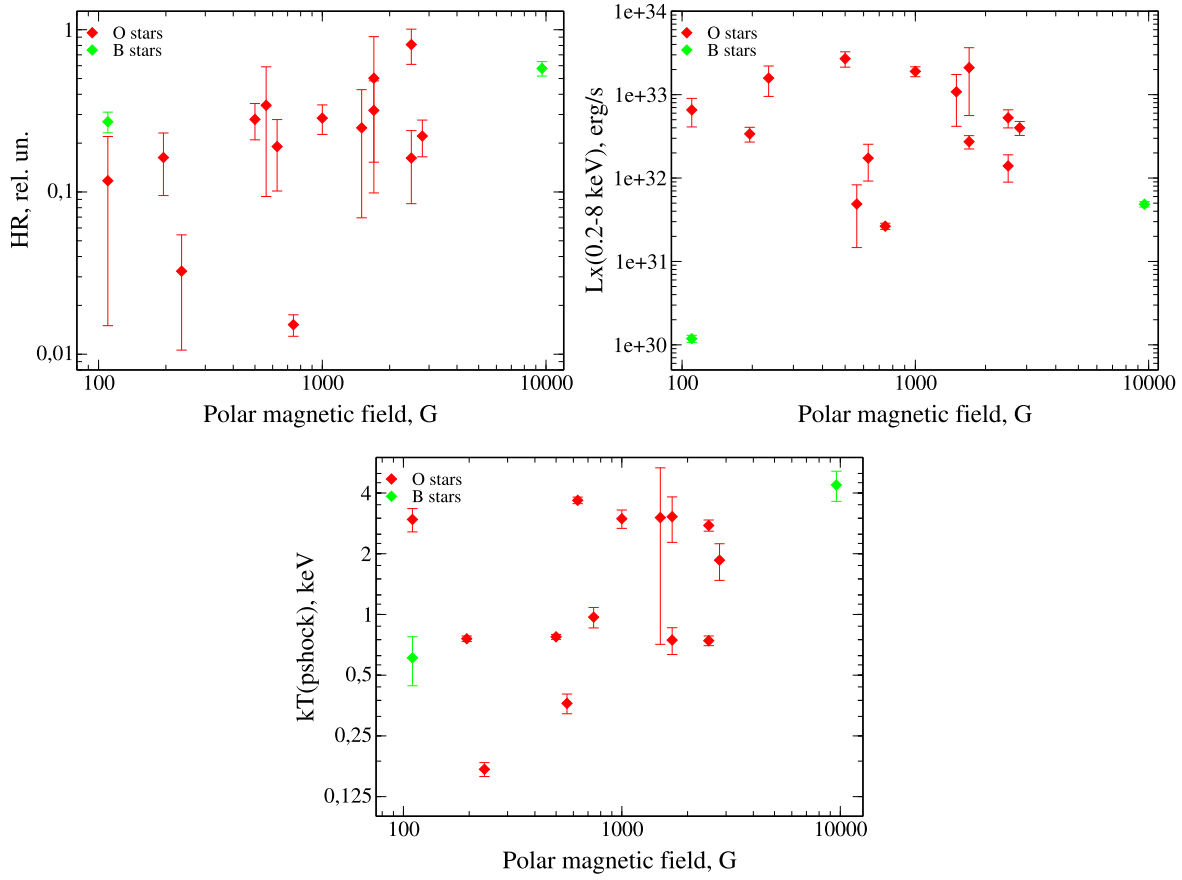
Figure 7. The correlations of the hardness ratio (top left panel), X-ray luminosity (top right panel) and plasma temperature of the PSHOCK component (bottom panel) with the polar magnetic field for the APEC+PSHOCK model fit.
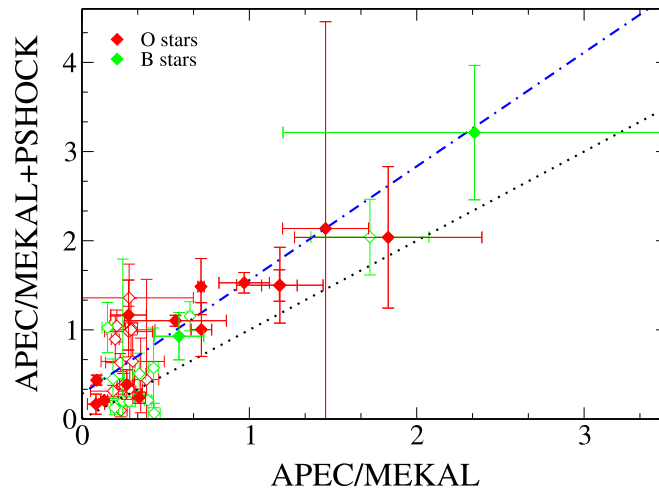

Figure 8. Comparison of average plasma temperatures from spectral fits by APEC/MEKAL and APEC/MEKAL+PSHOCK models. Black dotted line shows equal values, while blue dash-dotted line delineates a linear approximation (see text). Stars with magnetic fields and nonmagnetic stars are indicated by filled and empty symbols respectively.

Table 9
The Postshock Electron Number Density n_e and the Characteristic time T_{char} Inferred from PSHOCK+PSHOCK fit. Parameters Calculated from EM_1 and EM_2 indicated by (1) and (2) Respectively

Star	n_e 10^{11} cm^{-3} (1)	T_{char} s (1)	n_e 10^{11} cm^{-3} (2)	T_{char} s (2)	Star	n_e 10^{11} cm^{-3} (1)	T_{char} s (1)	n_e 10^{11} cm^{-3} (2)	T_{char} s (2)
CPD-282561	19.75 ± 14.66	0.51 ± 0.47	4.50 ± 0.77	0.78 ± 0.56	BD+433654	13.58 ± 8.13	5 ± 5	3.76 ± 1.21	11 ± 10
HD 101205	4.82 ± 0.39	0.84 ± 0.22	3.49 ± 0.28	1 ± 0	HD 97434	4.34 ± 2.22	3 ± 2	2.03 ± 0.30	4 ± 2
HD 108	24.11 ± 3.85	0.25 ± 0.16	6.72 ± 0.46	0.82 ± 0.49	HD 17505	2.37 ± 0.46	1 ± 1	1.08 ± 0.40	4 ± 3
HD 148937	5.72 ± 0.26	0.99 ± 0.15	5.52 ± 0.13	1 ± 0	HD 10144	0.09 ± 0.07	212 ± 189	0.036 ± 0.003	181 ± 90
HD 152233	13.36 ± 1.83	2 ± 1	3.95 ± 0.18	6 ± 3	HD 143275	0.14 ± 0.03	65 ± 45	0.12 ± 0.01	68 ± 43
HD 152249	5.16 ± 1.39	0.22 ± 0.12	1.16 ± 0.12	0.88 ± 0.35	HD 144217	0.66 ± 0.02	18 ± 6	0.34 ± 0.01	35 ± 11
HD 15558	4.31 ± 0.49	0.52 ± 0.24	2.27 ± 0.31	1.00 ± 0.47	HD 152234	3.41 ± 0.24	2 ± 0	2.27 ± 0.56	3 ± 1
HD 15570	11.48 ± 5.57	2 ± 1	4.92 ± 0.79	2 ± 2	HD 157246	1.46 ± 1.03	14 ± 12	0.69 ± 0.03	12 ± 5
HD 167971	3.41 ± 0.24	1 ± 0	2.10 ± 0.12	2 ± 1	HD 200775	5.78 ± 1.24	1 ± 1	1.39 ± 0.06	4 ± 2
HD 191612	15.47 ± 1.77	0.20 ± 0.08	4.39 ± 0.20	0.69 ± 0.22	HD 37000	3.55 ± 1.25	0.79 ± 0.62	0.27 ± 0.07	9 ± 7
HD 215835	10.84 ± 5.07	24 ± 24	5.02 ± 1.24	37 ± 37	HD 46328	0.89 ± 0.08	6 ± 1	0.87 ± 0.01	6 ± 0
HD 36512	0.82 ± 0.22	3 ± 1	0.50 ± 0.11	5 ± 2	HD 64760	1.79 ± 0.54	3 ± 2	1.34 ± 0.08	3 ± 1
HD 47129	11.37 ± 1.56	0.16 ± 0.05	2.83 ± 0.13	0.62 ± 0.15	HD 79351	0.26 ± 0.01	174 ± 55	0.28 ± 0.02	161 ± 53
HD 54662	2.10 ± 0.82	5 ± 3	1.41 ± 0.40	6 ± 4	HD 147932	0.26 ± 0.02	20 ± 7	0.26 ± 0.02	20 ± 7
HD 54879	1.26 ± 0.61	10 ± 8	1.57 ± 0.22	5 ± 3	HD 63922	0.92 ± 0.23	3 ± 1	0.50 ± 0.02	4 ± 1
HD 57682	2.31 ± 0.62	21 ± 18	2.21 ± 0.71	23 ± 20	HD 83953	0.05 ± 0.02	763 ± 614	0.26 ± 0.02	92 ± 53
HD 93128	6.47 ± 1.88	0.67 ± 0.46	3.86 ± 0.57	0.98 ± 0.60	HD 24398	0.94 ± 0.47	12 ± 9	0.61 ± 0.06	12 ± 6
HD 93129	29.27 ± 4.35	0.05 ± 0.01	10.16 ± 0.23	0.13 ± 0.02	ALS18058	0.21 ± 0.06	18 ± 12	0.18 ± 0.03	19 ± 11
HD 93205	12.02 ± 2.32	0.12 ± 0.05	3.72 ± 0.47	0.36 ± 0.12	HD 287848	0.17 ± 0.01	222 ± 70	0.24 ± 0.01	153 ± 47
HD 93250	6.07 ± 0.56	0.65 ± 0.17	5.78 ± 0.20	0.67 ± 0.14	HD 18552	0.22 ± 0.04	180 ± 144	0.23 ± 0.06	178 ± 146
HD 93403	2.71 ± 0.19	2 ± 1	2.15 ± 0.00	3 ± 1					
Tr16-22	1.74 ± 0.70	8 ± 6	3.05 ± 0.31	3 ± 2					

Table 10
The Same as in Table 9, but from APEC+PSHOCK Spectral Fits

| Star	n_e 10^{11} cm^{-3}	T_{char} s	Star	n_e 10^{11} cm^{-3}	T_{char} s
CPD-282561	0.24 ± 0.02	56 ± 52	BD-145040	0.26 ± 0.02	1 ± 1
HD 101205	1.52 ± 0.11	2 ± 1	BD+433654	0.51 ± 0.05	2 ± 1
HD 108	2.62 ± 0.27	3 ± 2	HD 97434	0.031 ± 0.004	191 ± 99
HD 148937	17.48 ± 1.21	(5.93 ± 1.68)·10^{-4}	HD 17505	0.62 ± 0.11	0.29 ± 0.20
HD 152233	14.79 ± 1.86	0.37 ± 0.23	HD 10144	0.41 ± 0.21	21 ± 21
HD 152249	0.029 ± 0.002	2 ± 1	HD 120324	0.53 ± 0.14	9 ± 7
HD 15558	5.43 ± 0.62	0.12 ± 0.04	HD 144217	0.39 ± 0.02	0.22 ± 0.04
HD 15570	0.43 ± 0.07	0.02 ± 0.01	HD 152234	1.22 ± 0.20	1 ± 0
HD 155806	0.16 ± 0.05	8 ± 6	HD 157246	1.65 ± 0.08	3 ± 1
HD 159176	1.14 ± 0.23	2 ± 1	HD 193924	0.47 ± 0.33	54 ± 54
HD 167971	9.61 ± 0.66	0.38 ± 0.11	HD 24760	5.23 ± 1.63	(8.59 ± 2.68)·10^{-4}
HD 191612	3.29 ± 0.08	0.96 ± 0.29	HD 33904	1.79 ± 0.10	(1.27 ± 0.28)·10^{-3}
HD 215835	2.73 ± 0.59	4 ± 3	HD 37479	0.37 ± 0.02	13 ± 8
HD 34078	5.34 ± 1.61	0.37 ± 0.26	HD 64760	4.34 ± 0.25	0.99 ± 0.29
HD 47129	6.09 ± 0.70	(1.02 ± 0.38)·10^{-3}	HD 63922	1.53 ± 0.14	12 ± 11
HD 47839	0.65 ± 0.04	3 ± 1	HD 83953	5.53 ± 0.38	4 ± 2
HD 54662	0.77 ± 0.39	43 ± 42	HD 24398	6.14 ± 0.56	1 ± 1
HD 54879	1.41 ± 0.15	5 ± 3	ALS18058	0.51 ± 0.12	0.21 ± 0.15
HD 57682	1.05 ± 0.25	37 ± 33	HD 287848	1.21 ± 0.04	81 ± 58
HD 93128	1.22 ± 0.37	3 ± 2	HD 287849	0.86 ± 0.08	4 ± 2
HD 93129	0.72 ± 0.02	0.11 ± 0.02	HD 18552	1.92 ± 0.46	6 ± 5
HD 93205	2.78 ± 0.29	0.32 ± 0.10			
HD 93250	0.13 ± 0.01	51 ± 25			
HD 93403	10.90 ± 0.75	0.46 ± 0.13			
HD 93521	0.08 ± 0.01	0.08 ± 0.03			
Tr16-22	0.15 ± 0.05	63 ± 61			
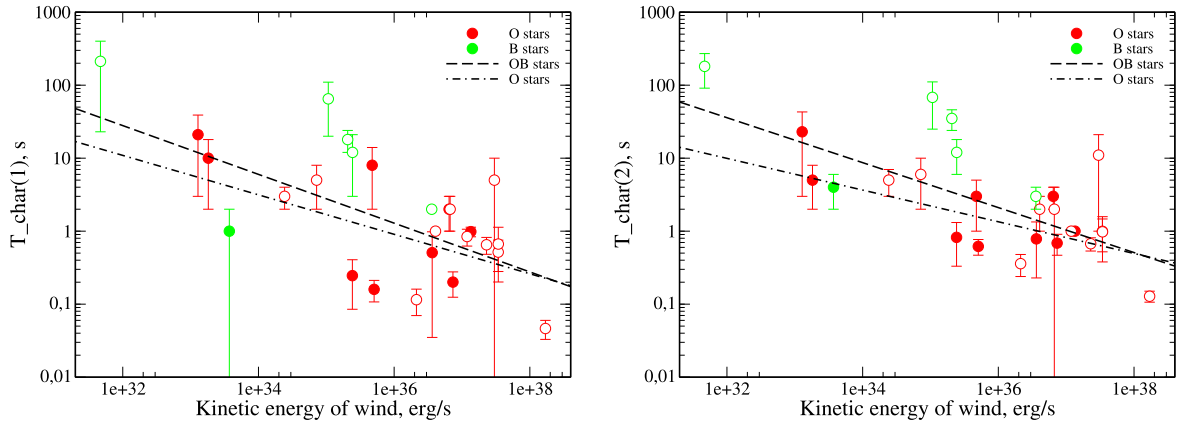
Figure 9. The dependence between parameter T_{char} and kinetic energy of stellar wind from spectral fits by the PSHOCK+PSHOCK model. Left panel shows dependencies for T_{char} from the first model component, while right panel features the same from the second component. Black lines indicate approximations. Stars with magnetic fields and nonmagnetic stars are indicated by filled and empty symbols respectively.
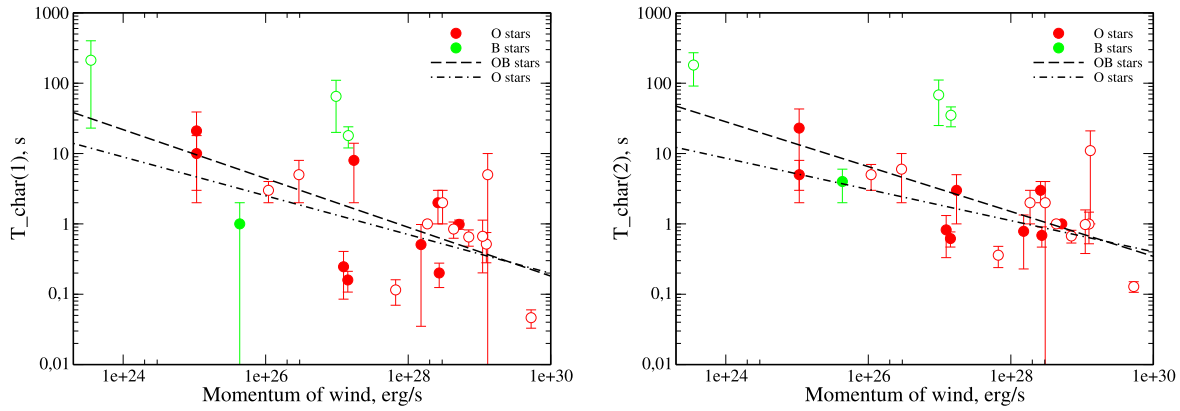

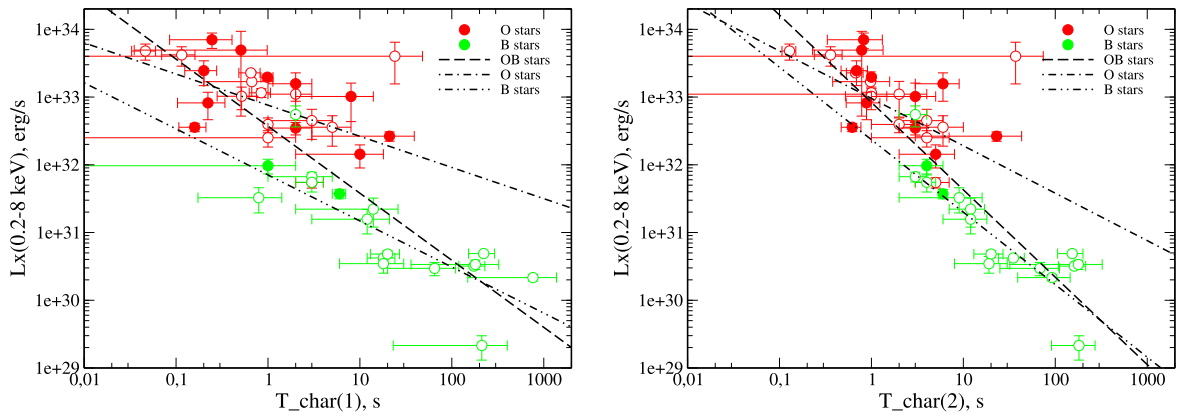**Figure 10.** The same as in Figure 9 for dependencies between T_{char} and momentum of wind.

Figure 11. The dependencies between unabsorbed X-ray luminosity and parameter T_{char} from spectral fits by the PSHOCK+PSHOCK model. Left and right panels demonstrate dependencies for T_{char} from the first and second model components respectively. Black lines indicate approximations. Stars with magnetic fields and nonmagnetic stars are indicated by filled and empty symbols respectively.

Table 11
The same as in Table 7, but for Dependences between X-ray Luminosities of Studied Stars, and Ionization Timescale τ_u and T_{char} Parameters

Approximation	Stars	Model	R	N	FAP	α	β
All examined stars							
$L_X(0.2\text{–}8\text{ keV}) = \alpha \cdot T_{char}(1)^{\beta}$	OB	2S	-0.82 ± 0.02	41	<0.001	$(5.48 \pm 4.04)\cdot10^{32}$	-0.99 ± 0.11
	O		-0.53 ± 0.13	24	<0.054	$(9.50 \pm 5.69)\cdot10^{32}$	-0.46 ± 0.18
	B		-0.75 ± 0.10	17	<0.005	$(1.06 \pm 0.78)\cdot10^{33}$	-0.68 ± 0.10
$L_X(0.2\text{–}8\text{ keV}) = \alpha \cdot T_{char}(2)^{\beta}$	OB	2S	-0.87 ± 0.05	41	<0.001	$(1.22 \pm 0.88)\cdot10^{32}$	-1.29 ± 0.18
	O		-0.56 ± 0.15	24	<0.048	$(1.19 \pm 0.71)\cdot10^{33}$	-0.71 ± 0.36
	B		-0.85 ± 0.03	17	<0.001	$(3.22 \pm 2.22)\cdot10^{32}$	-1.07 ± 0.10
$\tau_u = \alpha \cdot T_{char}(1)^{\beta}$	OB	2S	0.68 ± 0.09	42	<0.001	$(4.97 \pm 2.78)\cdot10^{11}$	0.31 ± 0.06
	O		0.71 ± 0.12	25	<0.002	$(6.87 \pm 4.63)\cdot10^{11}$	0.45 ± 0.18
	B		0.72 ± 0.10	17	<0.007	$(3.36 \pm 1.44)\cdot10^{11}$	0.34 ± 0.08
$\tau_u = \alpha \cdot T_{char}(2)^{\beta}$	OB	2S	0.61 ± 0.11	42	<0.001	$(4.19 \pm 2.33)\cdot10^{11}$	0.37 ± 0.08
	O		0.68 ± 0.17	25	<0.009	$(5.35 \pm 3.47)\cdot10^{11}$	0.56 ± 0.26
	B		0.66 ± 0.12	17	0.012 ± 0.011	$(2.35 \pm 0.77)\cdot10^{11}$	0.42 ± 0.12
$\tau_u = \alpha \cdot T_{char}^{\beta}$	OB	AS	0.78 ± 0.09	47	<0.001	$(1.95 \pm 1.63)\cdot10^{11}$	0.70 ± 0.17
	O		0.74 ± 0.07	30	<0.001	$(1.57 \pm 1.26)\cdot10^{11}$	0.63 ± 0.14
	B		0.83 ± 0.11	17	<0.001	$(2.78 \pm 2.45)\cdot10^{11}$	0.82 ± 0.25
Magnetic stars							
$L_X(0.2\text{–}8\text{ keV}) = \alpha \cdot T_{char}(2)^{\beta}$	OB	2S	-0.64 ± 0.12	13	0.036 ± 0.034	$(1.28 \pm 0.87)\cdot10^{33}$	-0.95 ± 0.43
$\tau_u = \alpha \cdot T_{char}(1)^{\beta}$	OB	2S	0.69 ± 0.08	13	0.014 ± 0.012	$(6.30 \pm 3.81)\cdot10^{11}$	0.39 ± 0.09
	O		0.73 ± 0.08	11	0.017 ± 0.014	$(7.73 \pm 5.30)\cdot10^{11}$	0.42 ± 0.13
$\tau_u = \alpha \cdot T_{char}(2)^{\beta}$	OB	2S	0.70 ± 0.14	13	<0.050	$(4.62 \pm 2.87)\cdot10^{11}$	0.61 ± 0.14
	O		0.80 ± 0.08	11	<0.01	$(5.39 \pm 3.66)\cdot10^{11}$	0.72 ± 0.26
$\tau_u = \alpha \cdot T_{char}^{\beta}$	OB	AS	0.76 ± 0.06	16	<0.002	$(1.85 \pm 1.54)\cdot10^{11}$	0.67 ± 0.18
	O		0.75 ± 0.06	15	<0.007	$(1.93 \pm 1.63)\cdot10^{11}$	0.67 ± 0.19
Nonmagnetic stars							
$L_X(0.2\text{–}8\text{ keV}) = \alpha \cdot T_{char}(1)^{\beta}$	OB	2S	-0.83 ± 0.01	28	<0.001	$(4.57 \pm 3.29)\cdot10^{32}$	-1.03 ± 0.11
	B		-0.72 ± 0.11	15	<0.014	$(9.96 \pm 7.80)\cdot10^{31}$	-0.65 ± 0.13
$L_X(0.2\text{–}8\text{ keV}) = \alpha \cdot T_{char}(1)^{\beta}$	OB	2S	-0.88 ± 0.05	28	<0.001	$(9.95 \pm 7.00)\cdot10^{32}$	-1.29 ± 0.16
	B		-0.83 ± 0.04	15	<0.001	$(3.29 \pm 2.47)\cdot10^{32}$	-1.05 ± 0.10
$\tau_u = \alpha \cdot T_{char}(1)^{\beta}$	OB	2S	0.71 ± 0.11	29	<0.001	$(4.52 \pm 2.55)\cdot10^{11}$	0.31 ± 0.05
	B		0.74 ± 0.09	15	<0.01	$(3.12 \pm 1.52)\cdot10^{11}$	0.36 ± 0.07
$\tau_u = \alpha \cdot T_{char}(2)^{\beta}$	OB	2S	0.62 ± 0.12	29	<0.006	$(3.99 \pm 2.28)\cdot10^{11}$	0.37 ± 0.08
	B		0.68 ± 0.11	15	<0.026	$(2.06 \pm 0.80)\cdot10^{11}$	0.45 ± 0.11
$\tau_u = \alpha \cdot T_{char}^{\beta}$	OB	AS	0.79 ± 0.11	31	<0.001	$(2.03 \pm 1.70)\cdot10^{11}$	0.73 ± 0.18
	O		0.71 ± 0.09	16	<0.01	$(1.37 \pm 1.06)\cdot10^{11}$	0.57 ± 0.10
	B		0.83 ± 0.11	15	<0.002	$(3.23 \pm 2.90)\cdot10^{11}$	0.83 ± 0.27

Table 12
The Same as in Table 11, but for Dependences between T_{char} from PSHOCK+PSHOCK fit and Parameters of Stellar Wind

| Approximation	Stars	R	N	FAP	α	β
All examined stars						
$T_{char}(1) = \alpha \cdot E_{kin}^{\beta}$	OB	-0.64 ± 0.05	26	<0.001	$(1.01 \pm 1.01)\cdot10^{14}$	-0.33 ± 0.06
	O	-0.55 ± 0.06	20	0.015 ± 0.001	$(3.72 \pm 3.72)\cdot10^{11}$	-0.27 ± 0.06
$T_{char}(2) = \alpha \cdot E_{kin}^{\beta}$	OB	-0.69 ± 0.01	26	<0.001	$(2.18 \pm 2.16)\cdot10^{12}$	-0.31 ± 0.03
	O	-0.62 ± 0.01	20	<0.006	$(3.72 \pm 3.72)\cdot10^{9}$	-0.22 ± 0.05
$T_{char}(1) = \alpha \cdot F_{M}^{\beta}$	OB	-0.63 ± 0.04	24	<0.003	$(1.29 \pm 1.29)\cdot10^{11}$	-0.35 ± 0.06
	O	-0.54 ± 0.05	20	0.02 ± 0.01	$(1.07 \pm 1.06)\cdot10^{9}$	-0.28 ± 0.06
$T_{char}(2) = \alpha \cdot F_{M}^{\beta}$	OB	-0.68 ± 0.01	24	<0.001	$(6.40 \pm 6.27)\cdot10^{9}$	-0.32 ± 0.03
	O	-0.601 ± 0.004	20	<0.006	$(2.87 \pm 2.87)\cdot10^{7}$	-0.22 ± 0.05
Nonmagnetic stars						
$T_{char}(1) = \alpha \cdot E_{kin}^{\beta}$	OB	-0.78 ± 0.01	16	<0.001	$(4.00 \pm 4.00)\cdot10^{17}$	-0.43 ± 0.06
$T_{char}(2) = \alpha \cdot E_{kin}^{\beta}$	OB	-0.82 ± 0.04	16	<0.001	$(4.69 \pm 3.79)\cdot10^{15}$	-0.41 ± 0.01
$T_{char}(1) = \alpha \cdot F_{M}^{\beta}$	OB	-0.75 ± 0.01	14	<0.003	$(4.02 \pm 4.02)\cdot10^{13}$	-0.43 ± 0.06
$T_{char}(2) = \alpha \cdot F_{M}^{\beta}$	OB	-0.78 ± 0.04	14	<0.002	$(1.79 \pm 1.30)\cdot10^{12}$	-0.42 ± 0.01
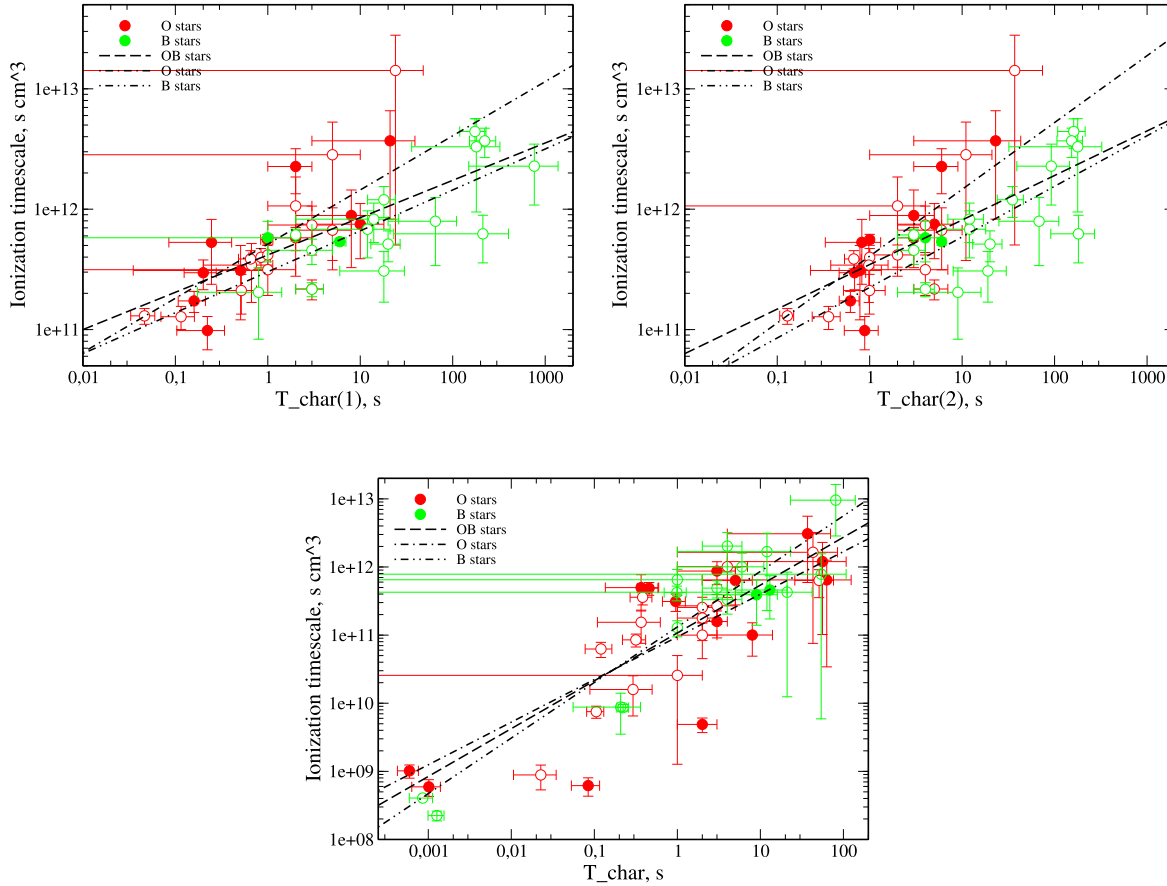
Figure 12. The dependencies between spectral parameters τ_u vs. T_{char}. Left and right top panels demonstrate dependencies for T_{char} from the first and second model components of fits by PSHOCK+PSHOCK respectively. Bottom panel displays dependencies from APEC+PSHOCK fit. Black lines indicate approximations. Stars with magnetic fields and nonmagnetic stars are indicated by filled and empty symbols respectively.

plasma cooling in local magnetic fields or for collision for fluxes of stellar winds. In both cases, the unit of plasma area cools faster in stars with strong winds and high X-ray luminosities. T_{char} does not depend on stellar magnetic field strength.

References

Anders, E., & Grevesse, N. 1989, Geochim. Cosmochim. Acta, 53, 197
Antokhin, I. I., Kholtygin, A. F., & Cherepashchuk, A. M. 1988, AZh, 65, 558
Babel, J., & Montmerle, T. 1997, Astronomy and Astrophysics, 323, 121
Balucinska-Church, M., & McCammon, D. 1992, ApJ, 400, 699
Borkowski, K. J., Lyerly, W. J., & Reynolds, S. P. 2001, ApJ, 548, 820
Capitanio, L., Lallement, R., Vergely, J. L., Elyajouri, M., & Monreal-Ibero, A. 2017, A&A, 606, A65
Cassinelli, J. P., Ignace, R., Waldron, W. L., et al. 2008, ApJ, 683, 1052
Cassinelli, J. P., & Swank, J. H. 1983, ApJ, 271, 681
Cherepashchuk, A. M. 1976, SvAL, 2, 138
De Becker, M., del Valle, M. V., Romero, G. E., Peri, C. S., & Benaglia, P. 2017, MNRAS, 471, 4452
De Becker, M., & Raucq, F. 2013, A&A, 558, A28
Feldmeier, A., Kudritzki, R. P., Palsa, R., Pauldrach, A. W. A., & Puls, J. 1997, A&A, 320, 899
Gudennavar, S. B., Bubbly, S. G., Preethi, K., & Murthy, J. 2012, ApJS, 199, 8
Hillier, D. J., Kudritzki, R. P., Pauldrach, A. W., et al. 1993, A&A, 276, 117
Ignace, R., Waldron, W. L., Cassinelli, J. P., & Burke, A. E. 2012, ApJ, 750, 40
Liedahl, D. A., Osterheld, A. L., & Goldstein, W. H. 1995, ApJL, 438, L115
Lucy, L. B. 1982, ApJ, 255, 286
Lucy, L. B., & White, R. L. 1980, ApJ, 241, 300
Mewe, R., Gronenschild, E. H. B. M., & van den Oord, G. H. J. 1985, A&AS, 62, 197
Mewe, R., Lemen, J. R., & van den Oord, G. H. J. 1986, A&AS, 65, 511
Morrison, R., & McCammon, D. 1983, ApJ, 270, 119
Nazé, Y., Petit, V., Rinbrand, M., et al. 2014, ApJS, 215, 10
Oskinova, L. M. 2016, AdSpR, 58, 739
Owocki, S. P., Castor, J. I., & Rybicki, G. B. 1988, ApJ, 335, 914
Runacres, M. C., & Owocki, S. P. 2002, A&A, 381, 1015
Ryspaeva, E., & Kholtygin, A. 2018, RAA, 18, 104

Ryspaeva, E., & Kholtygin, A. 2019, RAA, 19, 120
Ryspaeva, E., & Kholtygin, A. 2020, RAA, 20, 108
Ryspaeva, E., Kholtygin, A., & Lyutikov, M. 2023, MNRAS, 521, 2427
Smith, R. K., Brickhouse, N. S., Liedahl, D. A., & Raymond, J. C. 2001, ApJL, 556, L91
ud-Doula, A., & Nazé, Y. 2016, AdSpR, 58, 680

ud-Doula, A., Owocki, S., Townsend, R., Petit, V., & Cohen, D. 2014, MNRAS, 441, 3600
ud-Doula, A., & Owocki, S. P. 2002, ApJ, 576, 413
Walborn, N. R. 1972, AJ, 77, 312
Waldron, W. L., & Cassinelli, J. P. 2009, ApJL, 692, L76
Wilms, J., Allen, A., & McCray, R. 2000, ApJ, 542, 914